

UC Santa Cruz

UC Santa Cruz Previously Published Works

Title

Giant Outer Transiting Exoplanet Mass (GOT 'EM) Survey. V. Two Giant Planets in Kepler-511 but Only One Ran Away

Permalink

<https://escholarship.org/uc/item/6mh6q5hg>

Journal

The Astronomical Journal, 169(5)

ISSN

0004-6256

Authors

Chachan, Yayaati
Dalba, Paul A
Thorngren, Daniel P
[et al.](#)

Publication Date

2025-05-01

DOI

10.3847/1538-3881/adbe2f

Copyright Information

This work is made available under the terms of a Creative Commons Attribution License, available at <https://creativecommons.org/licenses/by/4.0/>

Peer reviewed



Giant Outer Transiting Exoplanet Mass (GOT ‘EM) Survey. V. Two Giant Planets in Kepler-511 but Only One Ran Away

Yayaati Chachan^{1,2,3} , Paul A. Dalba¹ , Daniel P. Thorngren⁴ , Stephen R. Kane⁵ , Howard Isaacson^{6,7} , Eve J. Lee^{2,3,8} , Edward W. Schwieterman⁵ , Andrew W. Howard⁹ , and Matthew J. Payne¹⁰

¹ Department of Astronomy and Astrophysics, University of California, Santa Cruz, CA 95064, USA; yachachan@ucsc.edu

² Department of Physics and Trotter Space Institute, McGill University, 3600 rue University, H3A 2T8 Montréal, QC, Canada

³ Trotter Institute for Research on Exoplanets (iREx), Université de Montréal, Montréal, QC, Canada

⁴ Department of Physics & Astronomy, Johns Hopkins University, Baltimore, MD 21210, USA

⁵ Department of Earth and Planetary Sciences, University of California Riverside, 900 University Avenue, Riverside, CA 92521, USA

⁶ Department of Astronomy, University of California Berkeley, Berkeley, CA 94720, USA

⁷ Centre for Astrophysics, University of Southern Queensland, Toowoomba, QLD, Australia

⁸ Department of Astronomy and Astrophysics, University of California, San Diego, La Jolla, CA 92093, USA

⁹ Department of Astronomy, California Institute of Technology, Pasadena, CA 91125, USA

¹⁰ Harvard-Smithsonian Center for Astrophysics, 60 Garden Street, MS 51, Cambridge, MA 02138, USA

Received 2024 May 16; revised 2025 February 4; accepted 2025 March 5; published 2025 April 4

Abstract

Systems hosting multiple giant planets are important laboratories for understanding planetary formation and migration processes. We present a nearly decade-long Doppler spectroscopy campaign from the HIRES instrument on the Keck-I telescope to characterize the two transiting giant planets orbiting Kepler-511 on orbits of 27 days and 297 days. The radial velocity measurements yield precise masses for both planets: $0.100^{+0.036}_{-0.039}$ (2.6σ) and $0.44^{+0.11}_{-0.12}$ (4σ) Jupiter masses, respectively. We use these masses to infer their bulk metallicities (i.e., metal mass fraction 0.87 ± 0.03 and 0.22 ± 0.04 , respectively). Strikingly, both planets contain approximately 25–30 Earth masses of heavy elements but have very different amounts of hydrogen and helium. Envelope mass loss cannot account for this difference due to the relatively large orbital distance and mass of the inner planet. We conclude that the outer planet underwent runaway gas accretion while the inner planet did not. This bifurcation in accretion histories is likely a result of the accretion of gas with very different metallicities by the two planets or the late formation of the inner planet from a merger of sub-Neptunes. Kepler-511 uniquely demonstrates how giant planet formation can produce dramatically different outcomes even for planets in the same system.

Unified Astronomy Thesaurus concepts: Exoplanet formation (492); Extrasolar gaseous giant planets (509); Radial velocity (1332); Transit photometry (1709)

1. Introduction

One of the many interesting findings to come from the discovery and characterization of exoplanet systems in recent years is that multiplanet systems are common. This conclusion about planet multiplicity has been reached by transit and radial velocity (RV) alike (e.g., S. E. Thompson et al. 2018; M. L. Bryan et al. 2019; L. J. Rosenthal et al. 2021; W. Zhu 2022). Of multiplanet systems, those with multiple giants pose interesting questions about planetary formation and the evolution of the system as a whole. Each giant planet formed from the same protoplanetary disk, but a variety of initial conditions (e.g., Y. Miguel et al. 2011; K. I. Öberg et al. 2011), migration channels (e.g., P. Goldreich & S. Tremaine 1980; F. A. Rasio & E. B. Ford 1996; Y. Wu & N. Murray 2003; Y. Lithwick & S. Naoz 2011; J. N. Winn et al. 2011), and other potentially stochastic processes (e.g., D. Carrera et al. 2019) eventually produce the planetary system as it is observed today. By measuring the current orbital and physical properties of giant planets in multiplanet systems, we aim to disentangle these processes and better understand planet formation as a whole.

Multiplanet systems containing transiting exoplanets are a particularly interesting subset because they allow for the measurement of at least one of the planets' radii and thereby its bulk density. In the specific case of a giant exoplanet ($\gtrsim 4 R_{\oplus}$), the bulk composition can lend clues about the planet's heavy element abundance (e.g., T. Guillot et al. 2006), which in turn informs its formation and evolution (e.g., J. B. Pollack et al. 1996; O. Mousis et al. 2009; D. P. Thorngren et al. 2016; Y. Hasegawa et al. 2018). Having this constraint for all of the known giant planets in a particular system is especially valuable as a tool for investigating different accretion processes ongoing in the same system. According to the NASA Exoplanet Archive (R. L. Akeson et al. 2013), of the nearly 900 known multiplanet systems, well over 100 have at least one transiting giant planet but only a few dozen contain multiple giant transiting planets.¹¹

Recent simulations aimed at capturing the impact of disk gap formation on multiple forming giant planets have found that the diverse distribution of mass ratios between giant planets in the same system necessitates different accretion start times as well as some amount of truncation of runaway accretion by disk dispersal (C. Berge-Casealou et al. 2023). Runaway accretion can occur at different times in different locations with a protostellar disk owing to different disk conditions such as disk opacity, aspect ratio, surface density,



Original content from this work may be used under the terms of the [Creative Commons Attribution 4.0 licence](https://creativecommons.org/licenses/by/4.0/). Any further distribution of this work must maintain attribution to the author(s) and the title of the work, journal citation and DOI.

¹¹ <https://exoplanetarchive.ipac.caltech.edu>

etc. (e.g., M. Ikoma et al. 2001; B. Bitsch et al. 2018; Y. Chachan et al. 2021). In this way, mass measurements of multiple giant planets in the same system provide insight into the properties of the local disk in which they both formed.

Moreover, the final orbital distances of giant planets in multiplanet systems hold clues as to how the planets migrated and their initial disk properties, which is especially interesting for comparison with our own multi-giant-planet system. P. Griveaud et al. (2023) found that pairs of giant planets only migrate inward in low-viscosity disks and end up as “warm Jupiters,” in contrast to solar system-based theories that suggest that Jupiter and Saturn also migrated outward together (e.g., K. Tsiganis et al. 2005; K. J. Walsh et al. 2011).

In this work, we confirm and characterize the Kepler-511 system (KOI-289), which was previously known to contain two statistically validated giant planets (T. D. Morton et al. 2016; H. Valizadegan et al. 2022). Despite the fact that Kepler-511 b and Kepler-511 c have long orbital periods relative to other transiting exoplanets (297 days and 27 days, respectively), both planets transit their host star. Moreover, the factor of 11 difference in their orbital periods (5x in semimajor axis), is much larger than nearly all other well-characterized systems of multiple transiting giant exoplanets.

This work adds another chapter to the Giant Outer Transiting Exoplanet Mass (GOT ‘EM) Survey, which aims to measure the masses and radii of giant exoplanets on relatively long-period orbits (P. A. Dalba et al. 2021a, 2021b; C. R. Mann et al. 2023; P. A. Dalba et al. 2024). Well-characterized giant planets with orbital periods of 100 days or longer are intrinsically rare owing to their low transit probabilities and the practical difficulty in measuring their masses via Doppler spectroscopy. The GOT ‘EM survey aims to increase the sample size of planets in this parameter space in support of giant planet formation and evolution theories. To date, this survey has measured the masses and orbital ephemerides of nearly a dozen giant planets with orbital periods between 100 and 1000 days.

This paper is organized as follows. In Section 2, we describe transit observations of Kepler-511 from the Kepler spacecraft and follow-up spectroscopy from the Keck Observatory. In Section 3, we model the stellar and planetary properties of this system with EXOFASTv2 (J. D. Eastman et al. 2019) and exoplanet (D. Foreman-Mackey et al. 2021a). In Section 4, we present the results of the modeling and take a step further to estimate the bulk heavy element abundance of both planets. Interestingly, both planets have similar masses of heavy elements but their bulk metallicity is notably different. In Section 5, we propose theories for how Kepler-511 b and Kepler-511 c formed given their bulk metallicities. Finally, in Section 6, we summarize our analysis and primary findings.

2. Observations

In the following sections, we describe how all photometric and spectroscopic observations were collected and processed.

2.1. Photometric Data from Kepler

Kepler-511 was observed by the Kepler spacecraft (W. J. Borucki et al. 2010) in Quarters 0–17 (2009 May 2 to 2013 May 11). We downloaded the data from the Mikulski Archive for Space Telescopes using the `lightkurve` package (Lightkurve Collaboration et al. 2018). Most of the

data were acquired at long cadence (30 minutes), although some short cadence (1 minute) data were available in Quarters 6 and 7. When both types of data were available, we defaulted to using the short cadence.

We made use of the Pre-search Data Conditioning Simple Aperture Photometry (PDCSAP; J. M. Jenkins et al. 2010; J. C. Smith et al. 2012; M. C. Stumpe et al. 2012), which was detrended for various systematic noise sources, including dilution and the fraction of Kepler-511’s flux that is captured by the photometric aperture. The point-spread function of Kepler-511 was approximately 1 pixel in radius, and the photometric apertures were approximately 2–3 pixels in radius. Each Kepler pixel subtends $\sim 4''$. The dilution correction did not account for the nearby source at $3''26$ identified by later direct imaging (see Section 3.3). However, this source is approximately 7 mag fainter than Kepler-511, making its flux contribution negligible given Kepler’s photometric precision.

We show PDCSAP data containing the four transits of Kepler-511 b and several transits of Kepler-511 c in Figure 1. The only additional detrending applied to the PDCSAP flux at this stage was a simple outlier removal. The light curves showed low-frequency signals, likely due to stellar variability, but these were handled later in the modeling (Section 3). In total, Kepler observed four transits of Kepler-511 b and over 50 transits of Kepler-511 c.

The Kepler-511 system was included in the transit timing variation (TTV) analysis of T. Holczer et al. (2016). The average significance (i.e., measurement divided by uncertainty) of the TTVs in the transits of both planets was less than unity. As a result, we did not account for possible TTVs when modeling the ephemeris of the Kepler-511 planets.

For completeness, it is worth mentioning that the Transiting Exoplanet Survey Satellite (TESS) mission has also observed Kepler-511. However, at the time of writing, it has not observed any transits of Kepler-511 b. We choose not to include TESS data for Kepler-511 c owing to its lower photometric sensitivity relative to Kepler.

2.2. Spectroscopic Data from HIRES

We acquired 20 spectra of Kepler-511 from the W. M. Keck Observatory using the High Resolution Echelle Spectrometer (HIRES; S. S. Vogt et al. 1994) over a span of 8.5 yr between 2013 June and 2021 November. Precise RVs for hundreds of stars using the iodine cell with HIRES have been shown to have no systematic errors over 20 yr timescales (L. J. Rosenthal et al. 2021). 19 of these 20 spectra were acquired with a heated I_2 cell in the light path, which imprinted a set of reference spectral lines. These I_2 lines enable wavelength calibration and tracking of the instrument profile for each observation. In the forward model, the line spread function is modeled as a series of Gaussians. The full model includes the line spread function parameters, the star’s RV, wavelength solution, dispersion, and a few other noncritical variables. The spectrum is divided into 700 individual 2 \AA subsections of spectrum from roughly 5000 to 6200 \AA and the highest weight is assigned to the best-performing subsections. There are no identified chromatic or other systematic errors that cause linear trends.

The HIRES I_2 -in spectra were collected with the C2 decker, which spans $14''.0 \times 0''.87$ in the spatial and dispersion direction, respectively. The spectra have a resolution of 60,000 at 5500 \AA . The minimum, median, and maximum signal-to-noise ratio (S/N) per pixel at 5500 \AA are 51, 72, and 105. The other observation

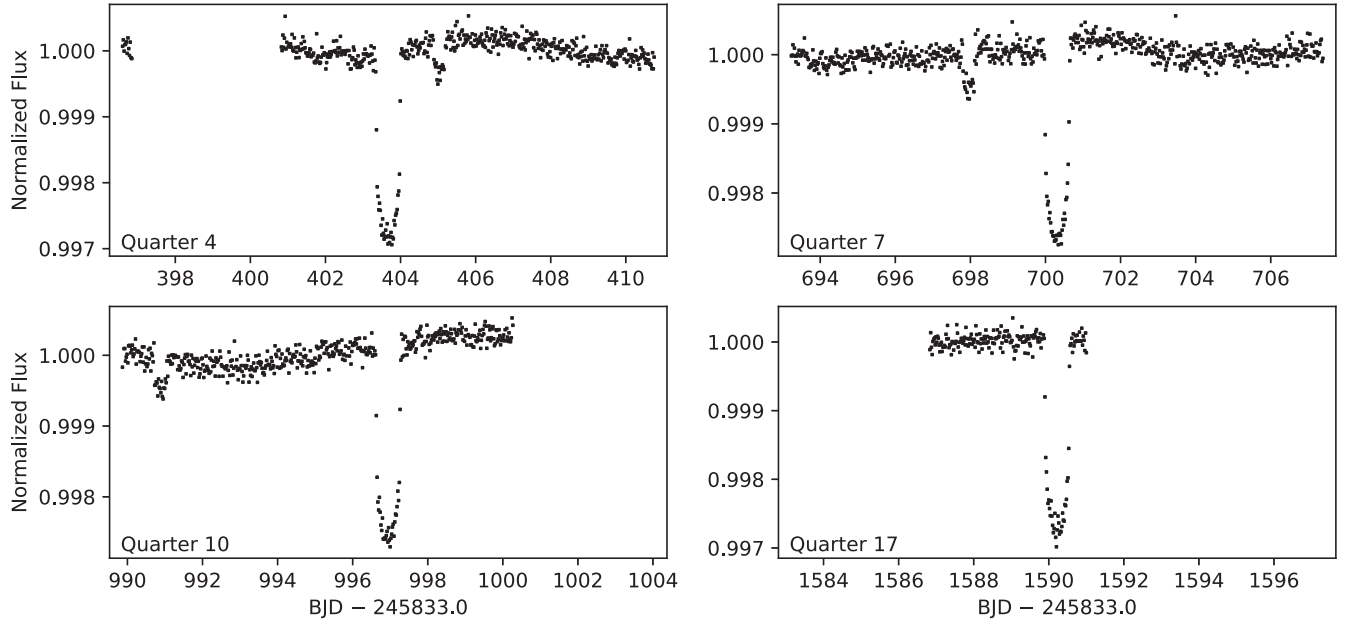


Figure 1. Raw Kepler photometry showing the four transits of Kepler-511 b and three of the transits of Kepler-511 c. Each panel is centered on the mid-transit time of Kepler-511 b and includes 10 transit durations worth of data before and after. Some baseline data were lost in all quarters except for Quarter 7, and the Quarter 14 transit was lost altogether to a data gap. Even in the raw light curves, the transits of both planets are visible. The stellar variability, which was removed prior to fitting the transit, can be seen as a gentle, low-frequency variation in flux.

was taken without the I_2 cell (decker dimensions $14.0'' \times 0.5''$) and had a higher S/N (126). This spectrum was used as a template in the forward modeling procedure that yielded the precise RV corresponding to each I_2 -in observation (R. P. Butler et al. 1996; A. W. Howard et al. 2010; B. J. Fulton et al. 2015). We limit the spectral extraction width to 14 pixels ($2.7''$) from the center of the star and as a result the ~ 8 mag fainter nearby star is not in the extracted spectrum (see Section 3.3). The precise RVs for Kepler-511 are listed in Table 1. The RV errors in Table 1 are internal errors from the I2-RV pipeline.

The wavelength coverage of HIRES (~ 360 – 900 nm) enables the measurement of the S_{HK} stellar activity indicator from the Ca II H and K lines (J. T. Wright et al. 2004; H. Isaacson & D. Fischer 2010). We include this indicator alongside the RVs in Table 1.

3. Modeling Kepler-511 System Parameters

3.1. Stellar Parameters

We processed the high S/N template spectrum (Section 2.2) of Kepler-511 with SpecMatch (E. A. Petigura et al. 2017) to determine its spectroscopic properties: stellar effective temperature $T_{\text{eff}} = 5855 \pm 100$ K, iron abundance $[\text{Fe}/\text{H}] = -0.36 \pm 0.06$ dex, surface gravity $\log g = 4.10 \pm 0.10$, and rotational velocity $v \sin i = 1.8 \pm 1.0$ km s $^{-1}$. We then treated these values of T_{eff} and $[\text{Fe}/\text{H}]$ as normal priors in an EXOFASTv2 fit between stellar evolution models and archival broadband photometry (J. Eastman et al. 2013; J. D. Eastman et al. 2019). The SpecMatch results were not used to place a prior on $\log g$ as it is only weakly constrained by spectroscopic data and placing such a prior on it can bias fitted stellar properties (G. Torres et al. 2012). We point the reader to J. D. Eastman et al. (2019) for a complete description of the EXOFASTv2 stellar evolution modeling. Briefly, EXOFASTv2 interpolates a grid of MIST isochrones (B. Paxton et al. 2011, 2013, 2015; A. Dotter 2016; J. Choi et al. 2016) and

Table 1
RV Measurements of Kepler-511 from Keck-HIRES

BJD _{TDB}	RV (m s $^{-1}$)	S_{HK}
2456449.90146	37.8 ± 3.2	0.137 ± 0.001
2456484.90839	36.3 ± 2.8	0.129 ± 0.001
2456513.84738	45.3 ± 3.0	0.128 ± 0.001
2456524.76180	21.7 ± 2.8	0.128 ± 0.001
2456532.79213	28.8 ± 2.6	0.129 ± 0.001
2457200.97212	33.1 ± 3.6	0.130 ± 0.001
2458294.92664	11.8 ± 3.4	0.137 ± 0.001
2458329.90056	-10.1 ± 3.6	0.132 ± 0.001
2458389.76351	2.9 ± 3.7	0.133 ± 0.001
2458632.87369	-18.1 ± 4.2	0.130 ± 0.001
2458714.89043	10.0 ± 3.3	0.128 ± 0.001
2458787.74592	-11.7 ± 3.8	0.122 ± 0.001
2459038.93765	8.9 ± 3.7	0.130 ± 0.001
2459099.87107	-20.2 ± 4.2	0.118 ± 0.001
2459296.13499	-19.2 ± 4.2	0.149 ± 0.001
2459421.02970	-33.1 ± 4.7	0.079 ± 0.001
2459445.99461	-41.3 ± 4.1	0.120 ± 0.001
2459470.84732	-40.0 ± 3.4	0.130 ± 0.001
2459546.76795	-45.2 ± 5.5	0.123 ± 0.001

precalculated bolometric corrections to derive basic stellar parameters and model the host star’s spectral energy distribution (SED). Our EXOFASTv2 fit included a uniform prior on reddening ($A_V \in [0, 0.19778]$) from galactic dust maps (E. F. Schlafly & D. P. Finkbeiner 2011) and parallax ($\varpi = 1.544 \pm 0.198$ mas) from Gaia Data Release 2 (DR; Gaia Collaboration et al. 2016, 2018). We also imposed noise floors on T_{eff} and bolometric flux consistent with the findings of J. Tayar et al. (2022) to account for systematic uncertainties in the MIST models and to avoid overconstraining our stellar—and thereby planetary—parameters. The EXOFASTv2 fit proceeded until convergence, which was assessed for each fitted parameter using the Gelman–Rubin statistic (<1.01) and the

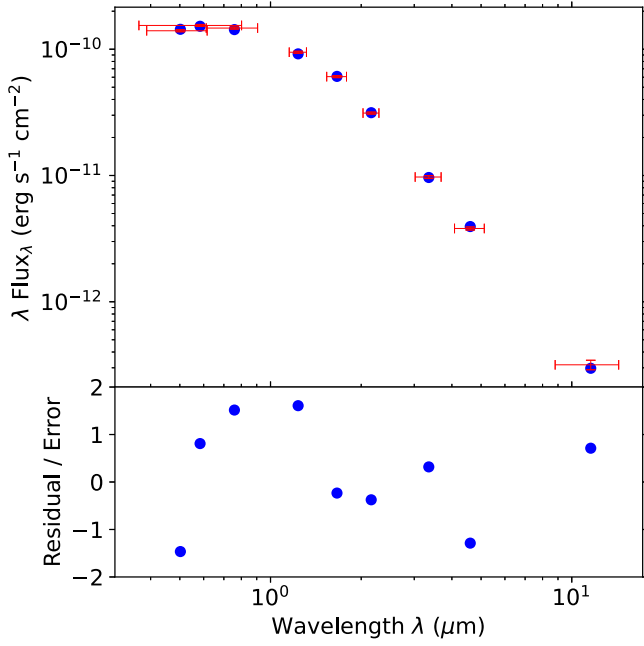


Figure 2. Top: the SED for Kepler-511 from 2MASS, Gaia, and WISE in red along with the maximum likelihood model from our EXOFASTv2 fit in blue. Bottom: residuals of the fit normalized by the uncertainties in the SED measurements.

number of independent draws from the posterior (>1000). The SED of Kepler-511 is shown in Figure 2. As is the default behavior for EXOFASTv2, the atmosphere model is not shown because this atmosphere was not used directly. Nonetheless, the residuals suggest that the fit is reasonable in each bandpass. The final stellar parameters are listed in Table 2. The fitted $\log g$ is compatible with the spectroscopic value at the 1.4σ level. We also verify that the fitted set of stellar parameters reproduces the star’s observed luminosity using a different grid of stellar models (PARSEC; A. Bressan et al. 2012).

Kepler-511’s luminosity and inferred stellar parameters imply that it is evolving off the main sequence. The broadband photometry of Kepler-511 indicates that the star is significantly more luminous than the Sun.¹² One potential confounding possibility for the source’s high luminosity is the presence of an unresolved companion. A. L. Kraus et al. (2016) reported a potential companion with a ΔK -band magnitude of 0.189 and a separation of $0''.017$ based on observations from NIRC2 on the Keck II telescope. Such a small K -band contrast requires the companion to be nearly equal mass and the small separation corresponds to a mere ~ 11 au in projected separation. The presence of such a binary companion would complicate our ability to place constraints on the properties of the two stars, and consequently, any planets around them (although the effect on planetary radii would be much smaller than the typical dilution correction; see the end of this section).

To resolve this issue, we closely examined various lines of evidence that support or reject the hypothesis of a nearby companion of Kepler-511.

¹² The exact luminosity does depend on the photometric points chosen for the fit. In their large-scale studies of planet-hosting stars, T. A. Berger et al. (2020) and T. A. Berger et al. (2023) chose 2MASS + SDSS g -band photometry and the Gaia G_{BP} and G_{RP} photometry for Kepler-511 and find that it is $2.75^{+0.20}_{-0.19}$ and $3.01^{+0.13}_{-0.12}$ times as luminous as the Sun, respectively. We use a wider range of photometric measurements for Kepler-511, which should provide a more reliable estimate of its stellar properties.

Table 2

Median Values and 68% Confidence Interval for Kepler-511 Stellar Parameters

Parameter	Units	Values
M_*	Mass (M_\odot)	$1.024^{+0.070}_{-0.060}$
R_*	Radius (R_\odot)	$1.785^{+0.063}_{-0.061}$
L_*	Luminosity (L_\odot)	3.49 ± 0.20
F_{bol}	Bolometric flux (cgs)	$2.66 \times 10^{-10} {}^{+1.5 \times 10^{-11}}_{-1.4 \times 10^{-11}}$
ρ_*	Density (cgs)	$0.253^{+0.035}_{-0.029}$
$\log g$	Surface gravity (cgs)	$3.945^{+0.044}_{-0.040}$
T_{eff}	Effective temperature (K)	5902^{+88}_{-86}
[Fe/H]	Metallicity (dex)	$-0.356^{+0.064}_{-0.060}$
[Fe/H] ₀	Initial metallicity ^a	$-0.264^{+0.082}_{-0.079}$
Age	Age (Gyr)	$7.5^{+1.7}_{-1.5}$
EEP	Equal evolutionary phase ^b	$456.7^{+3.3}_{-4.9}$
A_V	V-band extinction (mag)	$0.103^{+0.062}_{-0.066}$
σ_{SED}	SED error scaling	$1.49^{+0.59}_{-0.36}$
ϖ	Parallax (mas) ^c	1.544 ± 0.016
d	Distance (pc)	$647.8^{+6.8}_{-6.6}$

Notes. See Table 3 in J. D. Eastman et al. (2019) for a description of all parameters.

Catalog ID for Kepler-511: KOI-289, KIC-10386922, 2MASS J18514696 +4734295, Gaia DR3 2107644188496163200

^a The metallicity of the star at birth.

^b Corresponds to static points in a star’s evolutionary history. See A. Dotter (2016).

^c The fitted value is in good agreement with the Gaia DR3 parallax of 1.529 ± 0.010 .

1. We note that the reported detection pushed the resolving power of the NIRC2 instrument and that the companion has not been confidently recovered in follow-up imaging observations of the system (T. J. Dupuy et al. 2022; A. Kraus, private communication). This could be due to orbital motion.
2. However, the RV measurements of the star show a long-term trend of only $\sim 77 \text{ m s}^{-1}$ over the course of 8.5 yr. The presumptive nearly equal mass stellar companion would have to be on a highly improbable nearly face-on orbit to produce this relatively small RV trend. Such an orbit would also suggest that the companion should be detectable at other epochs, in contrast to follow-up observations.
3. The high-resolution template spectrum of the star obtained as part of the RV observations does not contain any hint of the presence of two stars and is well fitted by a single-star template (Appendix A; R. Kolbl et al. 2015). Stars with an RV separation of $\geq \pm 10 \text{ km s}^{-1}$ and flux level $>1\%$ of the primary are ruled out. If the binary companion is spectroscopically unresolved, we would expect the line profiles of the source to vary with time due to stellar orbital motion. However, the χ^2 and residuals of RV spectra fits do not exhibit any meaningful variation with epoch.
4. The Gaia RUWE value is merely 1.03 for Kepler-511, which is below the threshold of 1.4 that typically indicates the presence of an unresolved companion. The excess astrometric noise for Kepler-511 is 0.06 mas (4.8σ level). This is much smaller than what we would expect from a face-on nearly equal mass companion. Using the derived mass ($q = 0.983$) and luminosity ratios (adjusted to optical, $l \sim 1/1.3$) from

A. L. Kraus et al. (2016), we would expect the center of light to orbit around the center of mass (Z. Penoyre et al. 2020) with a separation of $|q - l|/(1 + q)/(1 + l) \times 17 \text{ mas} \sim 1.04 \text{ mas} \gg 0.06 \text{ mas}$. The astrometric noise is likely due to the presence of planets and a distant substellar companion around the star (Section 3.3). We also note that the astrometric excess noise may be higher in the early data releases from Gaia because it absorbs many different noise sources and that RUWE is a more reliable measure of the goodness of fit compared to the astrometric excess noise because RUWE is corrected for calibration error but astrometric excess noise is not (L. Lindegren et al. 2021).

5. The kinematic properties of the Kepler-511 system suggest that it is a member of the thick disk population with a thick-to-thin disk membership probability ratio of ~ 800 (D.-C. Chen et al. 2021). This is compatible with the stellar age implied by isochrone fitting.

All of these considerations lead us to conclude that Kepler-511 is likely a slightly evolved single star rather than a nearly equal mass binary. If the system is a binary, both stars would still need to be slightly evolved since their combined luminosity $= 3.49 \pm 0.20 L_{\odot}$ and their luminosity ratio in the K band is 1.19. We can estimate the magnitude of a secondary star's effect on the planets' radii. In our case, the correction would be significantly smaller than one would naively assume because accounting for a binary companion changes both the radius and the flux of the planet-hosting star. If δ and $l = l_{\text{secondary}}/l_{\text{primary}} < 1$ are, respectively, the transit depth and the luminosity ratio of the two stars, and assuming the planets orbit the primary star (easily extendable to the converse case), the corrected transit depth would be

$$\delta_{\text{corrected}} = \delta_{\text{observed}} (1 + l). \quad (1)$$

To obtain the planet radius, we would multiply $\sqrt{\delta}$ with the primary star's radius R_{primary} :

$$\begin{aligned} R_{p,\text{corrected}} &= \sqrt{\delta_{\text{observed}} (1 + l)} R_{\text{primary}} \\ &= \sqrt{\delta_{\text{observed}} (1 + l)} \sqrt{\frac{L_{\text{total}}}{4\pi\sigma_{\text{SB}} T_{\text{primary}}^4 (1 + l)}} \\ &= \sqrt{\frac{\delta_{\text{observed}} L_{\text{total}}}{4\pi\sigma_{\text{SB}} T_{\text{primary}}^4}}, \end{aligned} \quad (2)$$

where L_{total} is the total luminosity of the system, T_{primary} is the effective temperature of the primary planet-hosting star, and σ_{SB} is the Stefan-Boltzmann constant. If T_{single} denotes the effective temperature of a single evolved star that accounts for the total observed luminosity, the ratio of the inferred planetary radii in the binary scenario vs the single star scenario would be $=(T_{\text{single}}/T_{\text{primary}})^2$. If the nearly equal mass companion is real and unresolved in photometric data, we expect $T_{\text{primary}} \sim T_{\text{single}}$ and therefore the effect of binarity on the planets' radii should be much smaller than the typical dilution correction of $\sqrt{1 + l}$. Continued RV monitoring and future direct imaging observations are essential for illuminating the nature of this system but until the presence of a luminous companion is vindicated, we proceed assuming that Kepler-511 is a single evolved star.

3.2. Planetary Parameters

We used *exoplanet* (D. Foreman-Mackey et al. 2021a) to jointly model the Kepler-511 transit and RV data. We

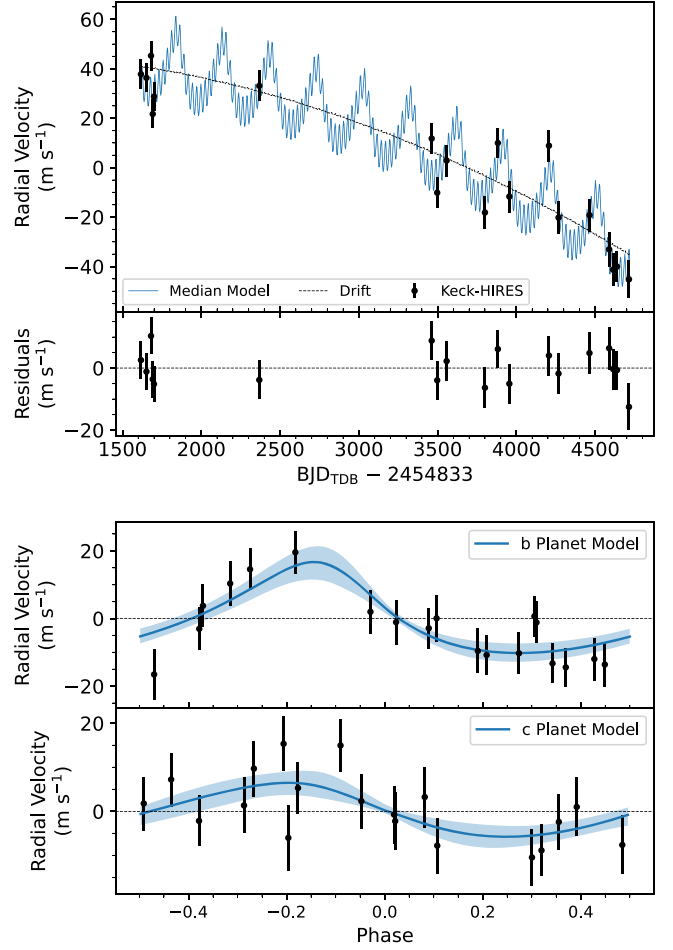


Figure 3. Top: time-series RV data from Keck-HIRES (black points) and median RV model (blue line). The need to include a long-term trend (dashed black line) in addition to the two planetary Keplerian signals is evident. The χ^2 of the RV model to the data (19 data points) with and without the RV jitter term is 15 and 45, respectively. Bottom: individual components of the RV for each planet folded on the best-fit ephemeris such that a phase of zero is the conjunction time (Table 3). The blue lines are the median models and the blue shaded regions are the 68% confidence intervals.

parameterized the transit models with the orbital period, the ratio between planetary and stellar radius, the stellar density, and quadratic limb-darkening parameters following D. M. Kipping (2013). We used our fit to the broadband photometry of the star to place a normal prior on the stellar density (Table 2) in our transit fit. A fit without a prior on the stellar density produced a higher likelihood ($\Delta\text{BIC} = 14$) and higher stellar density that agrees with the SED fitted value at the 2σ level. However, this difference in likelihood is driven entirely by the small number of RV data points, which biases the stellar density to higher values (see Appendix B). The normal prior on stellar density is therefore placed to alleviate this issue, in line with previous studies (N. Espinoza et al. 2019). The transit model also included a Gaussian process (GP) kernel corresponding to a damped simple harmonic oscillator meant to model the stellar variability signal in the photometry (e.g., D. Foreman-Mackey et al. 2021a). The short and long cadence data were treated with separate GP models, and only a subset of the Kepler data during and immediately surrounding the transits was fitted. For the RV model, we included terms for a quadratic trend, which were necessary based upon inspection of the time-series data (Figure 3, Section 3.3).

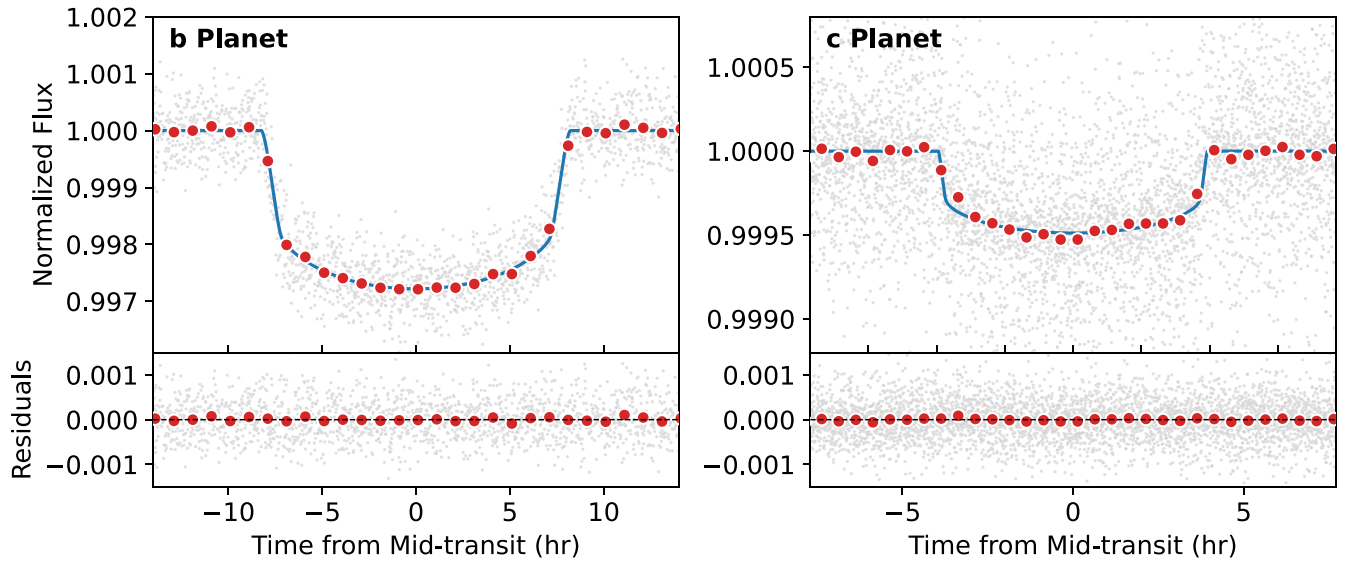


Figure 4. Kepler data and the median transit model, folded on the best-fit ephemeris (Table 3), for both Kepler-511 planets. Gray points represent individual frames, and red points are 1 and 0.5 hr bins for Kepler-511 b and Kepler-511 c, respectively. The rms error on the residuals is 414 ppm.

The exoplanet fit proceeded in two parts. First, there was an optimization of the fitted parameters to identify the local maximum a posteriori (MAP) point of the model. This MAP model included the GP for the photometry as well as the transits. We ran the MAP model several times, adjusting the starting points of the parameters and the order in which the parameters were optimized. Each time, we visually inspected the residuals with the transit and RV data until we were satisfied that the MAP solution was representative of the transit and RV data. We derived the photometric variation caused by stellar variability from this optimization and subtracted it from the transit light curves to effectively flatten the photometry. The stellar rotation period inferred via this maximum likelihood method was 25.1 days.

Second, we launched the Hamiltonian Monte Carlo routine to generate posterior predictive samples from the joint transit and RV model using the flattened photometry. The parameter estimation proceeded with 1500 tuning steps before making 6000 draws of the posterior. At that point, each fitted parameter had a Gelman–Rubin statistic of <1.01 and an effective sample size of $\gtrsim 1000$, which we took to demonstrate convergence.

The median transit models, folded on the ephemeris of each planet, are shown in Figure 4. The median and 68% confidence interval of the RV model are shown in Figure 3. The fitted parameters along with a few informative derived parameters are listed in Table 3. In deriving physical parameters from relative ones, we used the stellar properties and uncertainties listed in Table 2. Kepler-511 b and c have measured masses of $0.44^{+0.11}_{-0.12}$ (4σ) and $0.100^{+0.036}_{-0.039}$ (2.6σ) Jupiter masses, respectively.

3.3. A Distant Companion in Kepler-511 System?

Possibly adding to the peculiarity of the Kepler-511 system is the presence of a large RV drift ($\sim 77 \text{ m s}^{-1}$) present over the 8.5 yr observational baseline (Figure 3). This RV trend is unlikely to be due to stellar activity as its amplitude is larger than what one might expect from the activity (e.g., C. Lovis et al. 2011) and because there is little correlation (Pearson correlation coefficient of 0.35) between the RVs and the S_{HK} values measured from the Ca II H and K lines for the Keck-HIRES RVs

(Table 1; e.g., R. F. Díaz et al. 2016; R. P. Butler et al. 2017; L. J. Rosenthal et al. 2021).

The most plausible hypothesis for the cause of this trend is a distant companion orbiting far beyond Kepler-511 b. Such a companion would have important implications for the formation of the entire system, as planet–star and planet–planet interaction alike can excite the eccentricity of inner planets (e.g., Y. Wu & N. Murray 2003; Y. Lithwick & S. Naoz 2011). A direct imaging campaign with the NIRC2 instrument on the Keck II telescope that targeted Kepler-511 for resolved stellar companions claimed two detections (A. L. Kraus et al. 2016; E. Furlan et al. 2017): the first with a ΔK -band magnitude of 0.189 and separation of $0''.017$, and the second with a ΔK -band magnitude of 7.796 and separation of $3''.26$. We presented multiple lines of reasoning to argue that the closer imaged companion is a false positive in Section 3.1. Such a small K -band contrast would imply that this purported companion is nearly equal mass as the primary star. We rule out companions brighter than 1% of the primary’s brightness with RV separations of $\geq 10 \text{ km s}^{-1}$ (Appendix A). The observed RV trend would thus require the companion to be on a highly improbable face-on orbit. If it is on such an orbit, it should be detectable at multiple epochs but it has not been observed again since its initial detection (T. J. Dupuy et al. 2022). As for the companion at $3''.26$, recent Gaia astrometry identifies it as Gaia DR3 2107644188495101440, which is clearly not bound to Kepler-511 based on proper motion (Gaia Collaboration et al. 2023).

The RV drift shows significant curvature (the quadratic trend coefficient is nonzero at $\sim 4\sigma$ level), possibly suggesting that the observations sampled a portion of the distant companion’s orbit near quadrature and allowing us to draw useful constraints on the distant companion’s properties. We put constraints on the companion properties by subtracting the best-fit solutions for planets b and c from the RV data and fitting the residual long-term trend with *RadVel*. This procedure does not allow us to account for the covariance between the properties of the transiting planets and the distant companion. However, given the limited number of RV measurements, a three-planet fit is unfeasible due to the large number of free parameters. Our

Table 3
Median Values and 68% Confidence Interval for the Kepler-511 Planet Parameters

Parameter	Units	Values	
P	Period (days)	296.63766 ± 0.00039	26.629424 ± 0.000039
R_p	Radius (R_J)	0.886 ± 0.033	$0.371^{+0.018}_{-0.017}$
R_p	Radius (R_E)	9.93 ± 0.37	$4.16^{+0.20}_{-0.19}$
M_p	Mass (M_J)	$0.44^{+0.11}_{-0.12}$	$0.100^{+0.036}_{-0.039}$
M_p	Mass (M_E)	140^{+35}_{-38}	32^{+11}_{-12}
T_C	Time of conjunction (BJD _{TDB})	$2455236.67214^{+0.00083}_{-0.00082}$	2454971.7374 ± 0.0013
a	Semimajor axis (au)	0.894 ± 0.048	0.1792 ± 0.0097
i	Inclination (deg)	$89.719^{+0.029}_{-0.037}$	$88.59^{+0.38}_{-0.75}$
e	Eccentricity	$0.277^{+0.070}_{-0.068}$	$0.17^{+0.14}_{-0.11}$
ω_*	Argument of Periastron (deg)	26^{+19}_{-13}	18^{+89}_{-95}
T_{eq}	Equilibrium temperature ^a (K)	402 ± 14	899 ± 32
K	RV semi-amplitude (m s ⁻¹)	$13.7^{+3.4}_{-3.8}$	$6.8^{+2.4}_{-2.6}$
R_p/R_*	Radius of planet in stellar radii	$0.04986^{+0.00054}_{-0.00056}$	$0.02089^{+0.00066}_{-0.00061}$
a/R_*	Semimajor axis in stellar radii	107.6 ± 4.4	21.57 ± 0.89
δ	Transit depth (R_p/R_*) ^b	$0.002486^{+0.000054}_{-0.000056}$	$0.000436^{+0.000028}_{-0.000025}$
b	Transit impact parameter	$0.527^{+0.049}_{-0.066}$	$0.53^{+0.14}_{-0.28}$
ρ_p	Density (g cm ⁻³)	$0.84^{+0.23}_{-0.25}$	$2.6^{+1.0}_{-1.1}$
S_p	Insolation (S_{\oplus})	4.37 ± 0.54	109 ± 13
Kepler Limb-darkening Parameters:			
u_1	Linear coefficient	$0.524^{+0.097}_{-0.085}$	
u_2	Quadratic coefficient	$0.02^{+0.13}_{-0.14}$	
Keck-HIRES Parameters:			
γ	Relative RV offset ^b (m s ⁻¹)	$14.13^{+0.94}_{-0.96}$	
$\dot{\gamma}$	RV linear trend coefficient ² (m s ⁻¹ day ⁻¹)	$-0.0246^{+0.0015}_{-0.0014}$	
$\ddot{\gamma}$	RV quadratic trend coefficient ² (m s ⁻¹ day ⁻²)	$-0.0000047^{+0.0000012}_{-0.0000013}$	
σ_J	RV jitter (m s ⁻¹)	$5.1^{+1.8}_{-1.4}$	
Kepler Nuisance Parameters:		Short Cadence	Long Cadence
σ_F^2	Added flux variance (ppm)	$465.4^{+4.1}_{-4.0}$	95.6 ± 1.6
F_0	Baseline flux	1.0000 ± 0.0060	0.9999 ± 0.0029

Notes.

^a Assumes no albedo and perfect redistribution.

^b Relative to time BJD_{TDB} = 2457998.3347095.

constraints on the distant companion are likely to be tighter than the data merit but still useful for gauging the companion's properties and guiding follow-up RV campaigns. The top panel of Figure 5 shows the posteriors for the distant companion's semimajor axis, minimum mass ($M \sin i$), and eccentricity. The RV trend, best-fitting model, and 1000 sample models are shown in the bottom panel of Figure 5.

The distant companion in the Kepler-511 system may be planetary or stellar in nature. Given that we sample its orbit only partially, our constraints on its semimajor axis, mass, and eccentricity are highly correlated. Combinations of eccentricity and semimajor axis that lead to pericenter values (1, 5, and 10 au marked with red dashed lines in the top panel of Figure 5) close to the inner planets' orbits are implausible as they would violate the long-term stability of the system. These constraints also confirm our earlier analysis regarding the plausibility of a nearly equal mass stellar companion around Kepler-511: it would need to be on a nearly face-on orbit to match the observed RV trend. The distant companion is more likely to be a substellar object or a very low-mass star with a semimajor axis of ~ 10 – 100 au potentially on an eccentric orbit. Continued RV follow-up would be extremely useful for characterizing the properties of this companion and for understanding the context in which the inner planets formed and evolved.

4. The Kepler-511 Planets

Based upon the aforementioned photometric and spectroscopic data acquired from the Kepler-511 system, we find that Kepler-511 b and Kepler-511 c both have masses well within the planetary regime, thereby dynamically confirming them as genuine exoplanets. Figure 6 shows planets b and c in context with other planets in multiplanet systems that have measured masses and radii. Kepler-511 b joins the small but growing group of transiting cool giant exoplanets on orbits longer than ~ 100 days with precisely measured masses (e.g., P. A. Dalba et al. 2021a). Kepler-511 c presents as a dense Neptune-sized planet that may have a considerable gas envelope, just based on its mass and radius.

Among multiplanet systems, the Kepler-511 system is unique in that Kepler-511 c is significantly more massive than the inner super-Earths that typically accompany cold giants (e.g., W. Zhu & Y. Wu 2018; M. L. Bryan et al. 2019). In addition, Kepler-511 c is much smaller in size than planets of comparable mass in this multiplanet sample, indicating that it is not as gas-rich as other similar mass planets that accompany outer giants. The only other system that appears qualitatively similar to the Kepler-511 planets is the TOI-1130 system (L. Borsato et al. 2024, shown in purple in Figure 6), albeit at significantly shorter orbital periods). The combination of these properties makes the Kepler-511 system interesting from

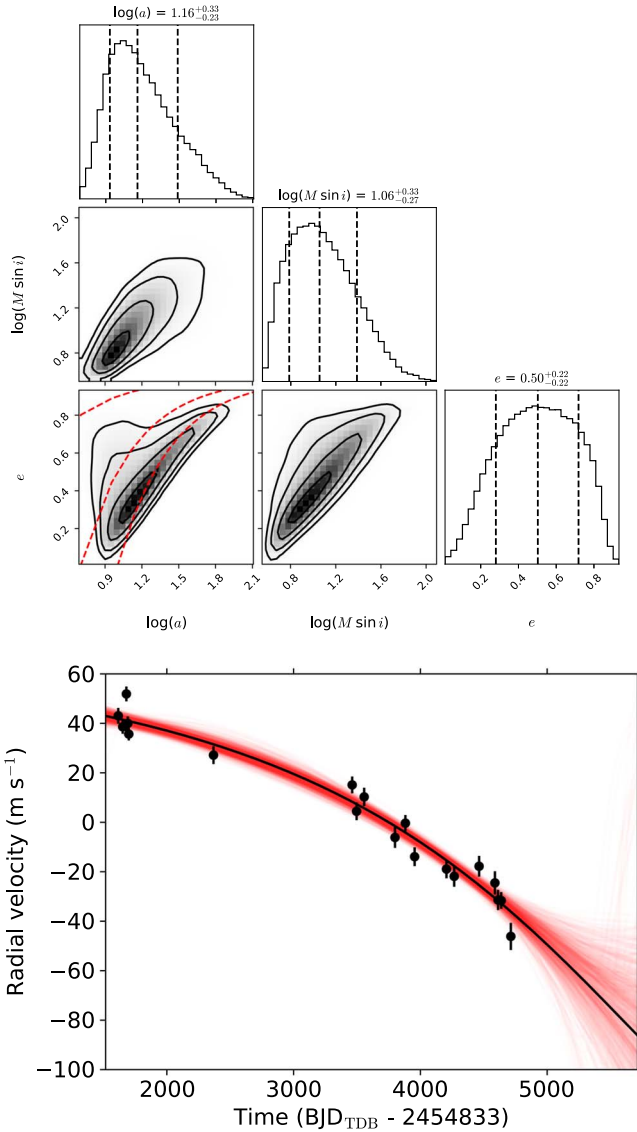


Figure 5. Top: corner plot for the constraints on the semimajor axis (AU), $M \sin i$ (M_{Jup}), and eccentricity of the distant companion. The red dashed lines in the eccentricity–semimajor axis 2D histogram mark pericenter values of 1, 5, and 10 au. Bottom: black points mark the RV data with the best-fit model for the two transiting planets subtracted out. The black curve shows the best-fit model to the long-term trend and the red curves correspond to 1000 models from randomly drawn parameters from the posterior.

a planet formation perspective. To explore the formation scenarios for the Kepler-511 planets further, we quantified the bulk heavy element content of both planets.

4.1. Planetary Bulk Metallicity

With a known mass, radius, and age for each planet in the Kepler-511 system, we retrieved the total mass of heavy elements that are possibly present within these planets (i.e., their bulk metal mass M_Z). We use a 1D planetary evolution model coupled to a radiative atmosphere model in order to evolve the radius of a giant planet along its cooling curve at a given mass. At the age of the system, we adjust M_Z to retrieve the known radius. The metals are assumed to be entirely in the core if $M_Z \leq 10 M_{\oplus}$. Any additional metal mass is incorporated into the envelope. For the model atmospheres, we use J. J. Fortney et al. (2007), a non-gray two-stream model at

solar metallicity, to determine the rate of heat flow out of the interior. The Kepler-511 planets are cool enough not to be affected by radius inflation. Additional details of this method and the models and assumptions used are reported by D. P. Thorngren et al. (2016) and D. Thorngren & J. J. Fortney (2019).

We found that the bulk metallicities ($Z_p \equiv M_Z/M_p$) of Kepler-511 b and c are 0.22 ± 0.04 ($Z_p/Z_{\star} = 35 \pm 8$) and 0.87 ± 0.03 ($Z_p/Z_{\star} = 143 \pm 20$), respectively. Figure 7 shows the posterior distributions for these metal retrievals and demonstrates that the fits are converged. Most parameters lack strong correlations with the exception of planet mass and metallicity for Kepler-511 c. In Kepler-511 c’s mass range, planet radius increases with mass for constant metallicity, and as a result, Kepler-511 c’s mass and metallicity are positively correlated to match the planet’s observed radius. Both planets are above the average of, although still consistent with, the correlation between relative bulk metallicity and giant planet mass identified by D. P. Thorngren et al. (2016).

Note that the uncertainties listed for the planet’s metallicity reflect only the statistical uncertainty arising from observational uncertainties in mass, radius, and age—they do not include theoretical uncertainty. The latter is difficult to quantify rigorously but the dominant sources are the structuring of metals within a planet (e.g., a core-dominated versus a well-mixed interior), uncertainties in the equations of state, and to a lesser extent our assumptions about how the planet has evolved thermally. For the first of these, moving metal from the envelope to the core in the model increases the inferred metallicity to some extent (see D. P. Thorngren et al. 2016, for further discussion of this modeling uncertainty). For equation-of-state uncertainties, those of H/He are the most important and in particular the calculation of their adiabats (Y. Miguel et al. 2016).

The measured bulk metallicities imply remarkably similar amounts ($31^{+12}_{-10} M_{\oplus}$ and $26^{+11}_{-10} M_{\oplus}$, respectively) of heavy elements in planets b and c despite the fact that they differ in mass by a factor of ~ 4.5 . This difference suggests that Kepler-511 b experienced runaway gas accretion while Kepler-511 c did not. Such a scenario is peculiar given that the ability of a planet to accrete gas is strongly dependent on the amount of heavy elements it contains. Despite having similar amounts of heavy elements, these planets have very different gas contents. This makes the Kepler-511 planets invaluable for studying giant planet formation history and gauging the role of other properties that control gas accretion.

It is interesting that two metal-enriched giant planets formed around such a metal-poor host star ($[\text{Fe}/\text{H}] = -0.36$) given the observed correlation between stellar metallicity and giant planet occurrence (e.g., D. A. Fischer & J. Valenti 2005). The combined metal mass in the two planets stretches the initial disk mass one needs for their formation around such a low metallicity star. Assuming (i) a 100% efficiency of converting dust to these planetary cores, (ii) the disk has the same metallicity as the host star, and (iii) a dust-to-gas mass ratio of 0.01 for a solar metallicity star, $57 M_{\oplus}$ of dust mass would require a gas disk that is at least 3.8% the mass of the host star ($1.024 M_{\odot} \times 0.01 \times 10^{-0.356} \times 0.038 \sim 57 M_{\oplus}$). Given that the efficiency of converting dust to planets is typically much smaller than 100% (e.g., J. Drazkowska et al. 2016; Y. Chachan & E. J. Lee 2023) and this estimate does not include the mass contained within the distant companion, the protostellar disk around Kepler-511 must have been $\gtrsim 10\%$ – 20% of the mass of the host star. Such a massive disk was likely prone to gravitational instability

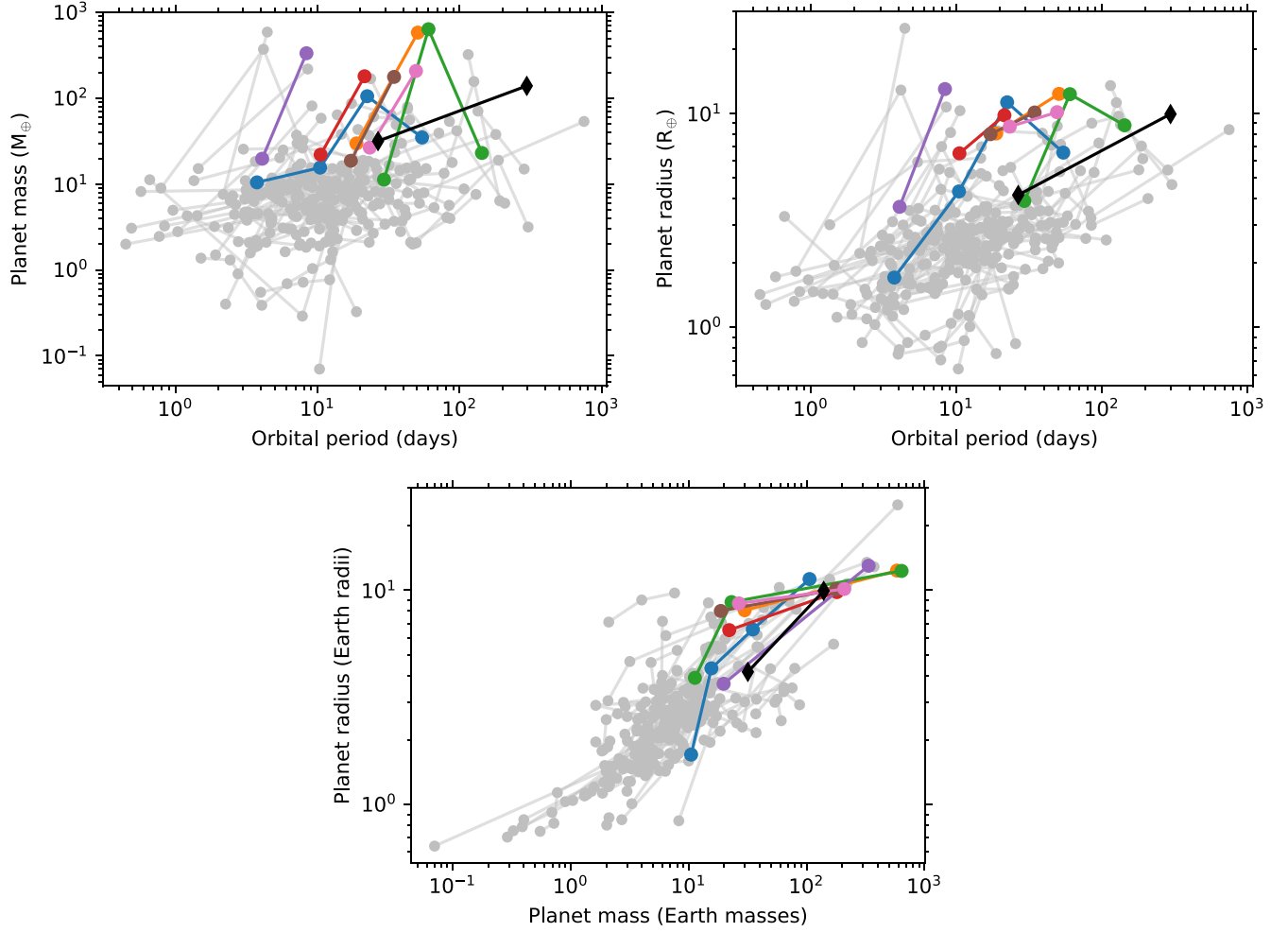


Figure 6. Multiplanet systems with planets that have measurements for both their masses and radii are shown (data from the exoplanet archive). Systems that do not have a single planet with mass $\geq 95M_{\oplus}$ or any planet with $17M_{\oplus} < \text{mass} < 95M_{\oplus}$ are grayed out. The Kepler-511 planets are shown with black diamonds. Kepler-511 b is the longest orbital period planet in such a sample. Gas-rich giants ($>95M_{\oplus}$) are typically accompanied by planets that are significantly less massive than Kepler-511 c. Some planets that do have masses similar to Kepler-511 c are typically much larger than it, indicating that they are much more gas-rich compared to Kepler-511 c.

(A. P. Boss 1997), which may have given birth to the star’s distant substellar companion. In the following section, we will consider how various theories of giant planet formation can explain the inferred bulk metallicities for the Kepler-511 planets.

5. Formation and Evolution Histories of the Kepler-511 Planets

The planets in the Kepler-511 system demonstrate the benefit of measuring precise masses and making bulk composition assessments for cool, giant exoplanets. Having only validated these planets (i.e., only measured their radii), our interpretation was limited to the fact that Kepler-511 is a system of multiple giant planets. By measuring masses and inferring their bulk metallicities, we can now conclude that these two sibling planets underwent different accretion processes during formation. In the following sections, we consider three broad explanations for how Kepler-511 b and Kepler-511 c formed and why they are so different from each other.

5.1. Envelope Mass-loss History

As the first explanation for the large composition difference between Kepler-511 b and c, we consider whether XUV-driven

mass loss could have removed a substantial portion of the inner planet’s envelope. Considering the XUV mass-loss models of E. D. Lopez et al. (2012, their Figure 5), a planet with a bulk density of 2.7 g cm^{-3} and receiving an irradiation of $\sim 110 S_{\oplus}$ should experience negligible mass loss on the order of $0.1 M_{\oplus} \text{ Gyr}^{-1}$ (0.3% of Kepler-511 c’s current total mass per Gyr). To verify and refine this approximate result, we applied the models of D. P. Thorngren et al. (2023) to Kepler-511 c. These models simulate the thermal and mass-loss evolution of giant planets using the stellar XUV evolution tracks of C. P. Johnstone et al. (2021) and the XUV-driven mass-loss models of A. Caldiroli et al. (2022).

For the planet’s structure, we adopt a core mass of $10 M_{\oplus}$ and adjust the envelope metallicity to 0.81 to match the observed radius (for a total $Z = 0.87$). Evolving forward from $0.101 M_J$, we estimate that the planet has lost just $0.194 M_{\oplus}$ of envelope material (0.67% of Kepler-511 c’s current total mass) over its $\sim 7.5 \text{ Gyr}$ lifetime. We find an insignificant present-day mass-loss rate of approximately $0.00906 M_{\oplus} \text{ Gyr}^{-1}$ (0.03% of Kepler-511 c’s current total mass). The estimates of mass loss are insensitive to the adopted core mass since the envelope metallicity will have to be adjusted accordingly to match the radius. For example, using a $25 M_{\oplus}$ core results in the loss of

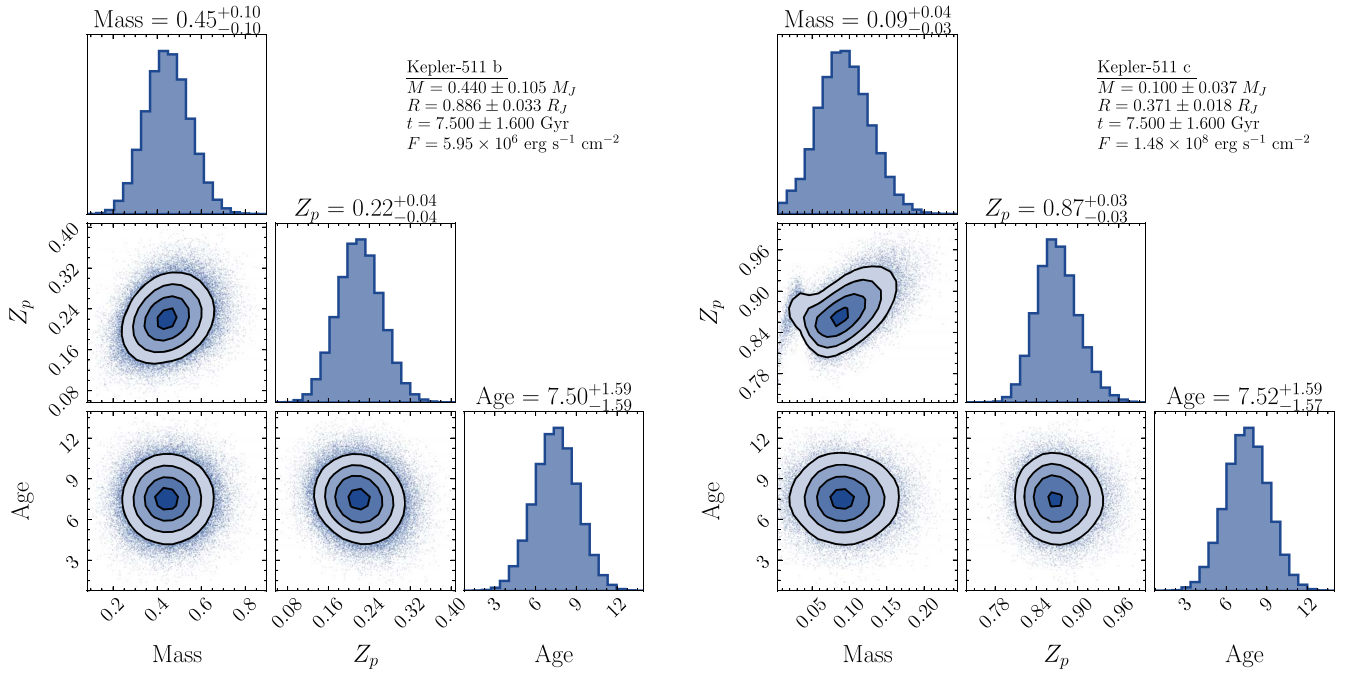


Figure 7. Posterior probability distributions for bulk metallicity (Z_p) retrievals for Kepler-511 b (left) and Kepler-511 c (right). For Kepler-511 b, the inferred values of Z_p do not show significant correlations with the measured planet masses or system age; for Kepler-511 c, mass, and Z_p are positively correlated to fit the planet’s observed radius (planet radius increases with mass at a constant metallicity in this planet mass range). By mass, Kepler-511 b and Kepler-511 c are 22% and 87% heavy elements.

$0.188 M_{\oplus}$ over the planet’s life. While the rate of mass loss may vary somewhat based on how active the star was in its early life (most of the mass loss occurs in the first couple Gyr), there is not a plausible value that would lead to substantial mass loss—the planet is simply too massive and distant from its parent star.

5.2. Differing Envelope Accretion Histories

The accretion of primordial envelopes is controlled by the mass of the planetary core, the metal content of the accreted gas, and to a lesser extent, the ambient nebular conditions (D. J. Stevenson 1982; R. R. Rafikov 2006; J.-M. Lee et al. 2014; A.-M. A. Piso et al. 2015). Given the remarkable similarities in the total metal content of the two planets, it is reasonable to first assume that the two planets had cores of similar masses. If the two cores are assumed to be $26 M_{\oplus}$ each, can differences in accreted material or nebular conditions account for their differing final masses and bulk densities? For this scenario to be plausible, Kepler-511 b must attain a gas-to-core mass ratio (GCR) of >0.5 and subsequently undergo runaway accretion, while Kepler-511 c only reaches a GCR of $\sim 1/6.7$ ($= (1 - Z_p)/Z_p$, assuming all the metals are in the core) before the dissipation of the protoplanetary disk. For such a scenario, we assume that the cores accreted for the same duration, which provides us with a useful limiting constraint on their accretion environment.

This difference is unlikely to be driven by differences in ambient gas density at the location of the two planets. The gas density at Kepler-511 c’s location would need to be a factor of $\sim 10^4$ lower compared to the density at Kepler-511 b’s location ($\text{GCR} \propto \Sigma^{0.12}$; E. J. Lee & N. J. Connors 2021), which would require Kepler-511 c’s $26 M_{\oplus}$ core to assemble only as the gas begins dissipating, which is similar to the merger scenario considered in Section 5.3. Gap opening is also unlikely to be

effective at creating such large gas density contrasts (assuming $M_p = 26 M_{\oplus}$, the gap depths would only differ by an order of magnitude for a factor of 2 difference in the disk aspect ratio, P. C. Duffell & A. I. MacFadyen 2013; J. Fung et al. 2014). We therefore focus on the formation of the Kepler-511 planets, assuming accretion of material with different dust content. The accretion of gas is mediated by the cooling of the planet’s envelope (E. J. Lee & E. Chiang 2015), which in turn depends on the opacity at the innermost radiative-convective boundary (RCB) of the envelope. The innermost RCB of envelopes that have even a small amount of dust ($\gtrsim 0.01$ solar metallicity for interstellar-medium-like size distribution) is set by the hydrogen dissociation front, inside which H^- opacity dominates. Metallic species accreted by a planet are the primary source of free electrons that create H^- ions, and a large difference in the local disk metallicity (as can be probed with dust content) could therefore produce the divergent accretion histories of the Kepler-511 planets (Y. Chachan et al. 2021).

Assuming both planets reached these GCRs in the same amount of time and that the temperature and the adiabatic index at their RCBs did not differ, we arrive at the following expression from E. J. Lee & N. J. Connors (2021):

$$\left(\frac{\Sigma_b}{\Sigma_c}\right)^{0.12} \left(\frac{Z_c}{Z_b}\right)^{0.4} \left(\frac{\mu_b}{\mu_c}\right)^{3.4} \gtrsim \frac{1/2}{1/6.7}, \quad (3)$$

where Σ is the gas surface density, Z is the dust-to-gas ratio or equivalently the dust content of the accreted material, μ is the mean molecular weight, and the subscripts correspond to the two planets. For $\Sigma \propto r^{-1}$, the ratio $\Sigma_b/\Sigma_c = a_c/a_b$, i.e., the inverse ratio of their semimajor axes. Since $1/\mu = Z/\mu_Z + (1 - Z)/\mu_{\text{H,He}}$ with $\mu_Z = 17$ (approximate mean molecular weight of metals in a solar metallicity gas at the relevant temperature and pressure, P. Woitke et al. 2018) and $\mu_{\text{H,He}} = 2.32$ (M. Asplund et al. 2021;

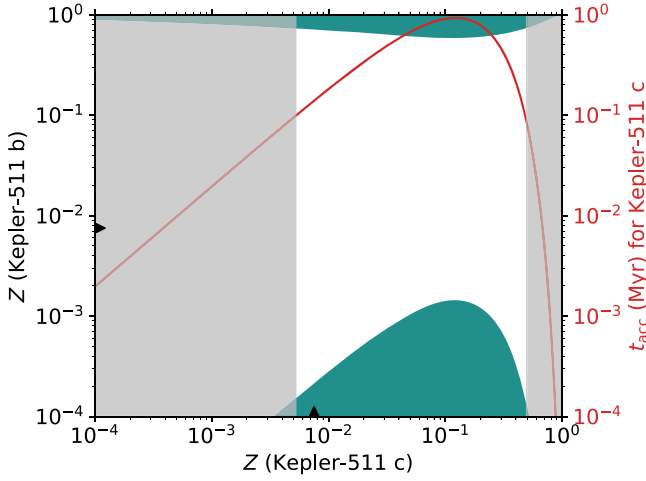


Figure 8. Bulk metallicity parameter space for Kepler-511 b (y-axis) and Kepler-511 c (x-axis). On both axes, the stellar metallicity is shown with the black triangles. The solid red line (corresponding to the right-side y-axis) shows the time (t_{acc} for Kepler-511 c to accrete its GCR of $\sim 1/6.7$). Grayed-out regions exclude scenarios whereby Kepler-511 c has $t_{\text{acc}} < 0.1$ Myr, which would require fine-tuning to prevent it from undergoing runaway gas accretion. The allowed regions of parameter space (green) suggest that Kepler-511 c accreted material with a higher metallicity than the host star. The metallicity of the material accreted by Kepler-511 b is likely lower than that of the host star, as the higher metallicity region is unrealistic.

K. Lodders 2021), this expression provides us with a preliminary estimate of the difference in Z required for Kepler-511 b to undergo runaway gas accretion while Kepler-511 c accretes a modest envelope:

$$\left(\frac{Z_c}{Z_b}\right)^{0.4} \left(\frac{1 - Z_c + (\mu_{\text{H,He}}/\mu_Z)Z_c}{1 - Z_b + (\mu_{\text{H,He}}/\mu_Z)Z_b}\right)^{3.4} \gtrsim \frac{1/2}{1/6.7} \left(\frac{a_b}{a_c}\right)^{0.12}. \quad (4)$$

The dust content that leads to the different formation outcomes for the Kepler-511 planets is marked in color in Figure 8. We estimate the time required for Kepler-511 c to reach a GCR of $1/6.7$ assuming $\Sigma_c = 2000 \text{ g cm}^{-3}$, adiabatic index of 0.17, and temperature of 2500 K at the RCB, and the planet’s effective accretion radius $f_R = 0.2$ times its Hill radius (E. J. Lee & N. J. Connors 2021):

$$\left(\frac{t_{\text{acc,c}}}{1 \text{ Myr}}\right)^{0.4} = \frac{\text{GCR}_c f_R^{-1}}{0.06} \left(\frac{Z}{0.02}\right)^{0.4} \left(\frac{2.37}{\mu}\right)^{3.4} \times \left(\frac{5M_{\oplus}}{M_{\text{core}}}\right)^{1.8} \left(\frac{2000 \text{ g cm}^{-2}}{\Sigma_c}\right)^{0.12}. \quad (5)$$

We gray out the parameter space in which Kepler-511 c accretes its envelope in less than 0.1 Myr to alleviate the issue of fine-tuning the gas dissipation timescale. Figure 8 shows that for Kepler-511 c, the dust content of the material accreted must be above the stellar value to sufficiently suppress gas accretion. For Kepler-511 b, the metallicity must either be much lower to speed up envelope cooling and accretion or so much higher that the high mean molecular weight of the accreted material expedites gas accretion. The high- Z_p region for Kepler-511 b can likely be ruled out because it is unrealistically high (>0.5).

The combination of high- Z for the inner Kepler-511 c and low- Z for the outer Kepler-511 b may be achieved if the two planets

were separated by the water snowline (Y. Chachan et al. 2021). This scenario has the caveat that the fragmentation velocities of ice-free grains need to be smaller than those of the icy grains, such that the smaller ice-free grains slow their radial drift and pile up in the inner disk, boosting the local Z there. However, the latest laboratory measurements suggest the material strength between these two types of grains may be more similar than previously thought (e.g., B. Gundlach et al. 2018; G. Musiolik & G. Wurm 2019; H. Kimura et al. 2020). Alternative mechanisms to alter the envelope opacity would require enhanced dust accretion onto Kepler-511 c due to the presence of disk substructures (e.g., Y.-X. Chen et al. 2020) or grain growth and expedited cooling in Kepler-511 b’s atmosphere (e.g., C. W. Ormel 2014; A.-M. A. Piso et al. 2015) to explain the different gas accretion histories for Kepler-511 b and c.

We briefly note that meridional flows that advect disk material within a planet’s Hill sphere could limit its envelope’s ability to cool and grow (C. W. Ormel et al. 2015; M. Ali-Dib et al. 2020; T. W. Moldenhauer et al. 2021). Studies that employ more realistic opacities and equations of state show that the effect of this recycling on envelope accretion is not as potent as initially supposed (Z. Zhu et al. 2021; A. Bailey & Z. Zhu 2024; V. Savignac & E. J. Lee 2024). The effect of recycling is also distance-dependent: in hotter regions of the disk close-in to the star, it can lead to a slowdown in gas accretion but the exact magnitude of the effect depends on the inner disk conditions (A. Bailey & Z. Zhu 2024; V. Savignac & E. J. Lee 2024). However, although these uncertainties might affect the amount of gas accreted by super-Earth mass cores, they are unlikely to prevent a $\sim 26 M_{\oplus}$ from accreting substantially more gas than Kepler-511 c possesses.

5.3. Kepler-511 c’s Formation by Giant Impacts of Sub-Neptunes

Since the two Kepler-511 planets have puzzling different accretion histories, we explore if this is an outcome of Kepler-511 c forming by mergers of two or three planets (sub-Neptunes) after the gas disk’s dispersal. It is more plausible that lower mass sub-Neptunes, rather than a $30 M_{\oplus}$ core, would accrete envelopes that are only $\sim 10\%$ of their mass. If these sub-Neptunes subsequently undergo a dynamical instability that leads to their coalescence into a planet such as Kepler-511 c, we could explain why Kepler-511 b turned into a gas giant while Kepler-511 c did not. This is similar to the hypothesis of late-stage formation of super-Earths (R. I. Dawson et al. 2016; E. J. Lee & E. Chiang 2016), except we primarily consider dynamical instabilities after gas dissipation when damping by the gas does not act to stabilize the system. Dynamical instability after the gas disk dispersal is in line with the results of F. Dai et al. (2024), who show that young (<100 Myr) multiplanet systems are almost always found to be resonant and that these resonances get disrupted over ~ 100 Myr timescale to produce the observed orbital period ratios of mature planetary systems. Such an explanation would also have the advantage of forming Kepler-511 c from inner planets that are akin to those observed around Sun-like stars, especially those interior to cold Jupiters (W. Zhu & Y. Wu 2018; M. L. Bryan et al. 2019). Given the age of the Kepler-511 system ($7.5^{+1.7}_{-1.5}$ Gyr), it is plausible that a typical inner system of sub-Neptunes became unstable and merged to form Kepler-511 c. An instability might arise if the eccentricities and/or mutual inclinations of the sub-Neptunes are excited to large enough values to lead to orbit crossing. These excitations may be a result of the planets’ mutual

interactions with each other or they may be driven by the outer Kepler-511 b (e.g., B. Pu & D. Lai 2018; S. T. S. Poon & R. P. Nelson 2020).

What causes instability in a tightly packed system of planets is an area of ongoing research. In general, the onset of chaos is attributed to the overlap of two-body mean-motion resonances and three-body resonances (J. Wisdom 1980; S. Hadden & Y. Lithwick 2018; A. C. Petit et al. 2020; C. Lammers et al. 2024). The time required for a tightly packed chain of sub-Neptunes to undergo mergers is exponentially sensitive to the orbital spacing between the planets, their orbital eccentricities, and their mutual inclinations (B. Pu & Y. Wu 2015). Since the mergers are typically pairwise, it is difficult to conceive of more than two or three planets all merging together to form Kepler-511 c. Therefore, we restrict our discussion to a system of three $10.5 M_{\oplus}$ sub-Neptunes. The extent to which Kepler-511 b can excite the inner planets' eccentricities and/or inclinations depends on the strength of their dynamical coupling, quantified by $\bar{\epsilon}$ as the ratio of the differential precession frequency of the inner planets with the outer giant and the mutual precession frequencies of the inner planets (B. Pu & D. Lai 2018). We find that for period ratios \mathcal{P} in the range of 1.2–2 for the inner sub-Neptunes, $\bar{\epsilon}$ varies from 10^{-3} to 10^{-1} . This implies that the inner sub-Neptunes would be more strongly coupled to each other than the outer giant and the giant planet alone is unlikely to drive the system to instability ($\bar{\epsilon} \gtrsim 1$ requires $\mathcal{P} \gtrsim 3.5$). Nonetheless, interactions with the outer giant planet can impart nonzero eccentricity to the inner sub-Neptunes and we use secular perturbation theory to calculate it (B. Pu & D. Lai 2018). The rms time-averaged eccentricity of the three sub-Neptunes normalized by the crossing eccentricity ($e_{\text{cross}} = (\mathcal{P}^{2/3} - 1)/(\mathcal{P}^{2/3} + 1)$) is shown in dashed white line as a function of the period ratio \mathcal{P} of the three sub-Neptunes in Figure 9.

We use SPOCK to determine the probability that a system of three sub-Neptunes with an outer giant planet is stable over timescales of 10^9 orbits (D. Tamayo et al. 2020). SPOCK uses REBOUND (H. Rein & S. F. Liu 2012) to integrate orbits of an input planet configuration over the first 10^4 orbits and measures summary statistics that are then used to predict stability probability from a machine-learning model trained on a set of $\sim 100,000$ scale-invariant simulations of three-planet systems. D. Tamayo et al. (2020) and N. Sopski & S. C. Millholland (2023) have shown that SPOCK generalizes well to planet configurations it was not trained on and that it agrees with prior stability metrics. We therefore adopt it to evaluate whether Kepler-511 c could have formed from mergers of a system of inner sub-Neptunes.

Period ratios \mathcal{P} of the inner sub-Neptunes are incremented by 0.01 in the range of 1.25–2 and their eccentricities are set as a fraction of the orbit crossing eccentricity (in increments of 0.05 in the range of 0–0.5). For each combination of \mathcal{P} and e , we calculate the stability probability for 100 different realizations of the arguments of pericenter and the initial mean anomalies (each randomly sampled from a $\mathcal{U}[0, 2\pi)$) and average them to obtain a mean estimate that is shown by color in Figure 9. The stability probability is lowest for \mathcal{P} , which corresponds to integer ratios, as expected from the near-resonant interactions of the inner sub-Neptunes. Higher eccentricities also lower the probability that the system is stable over long timescales. Eccentricity pumping due to secular interactions with Kepler-511 b therefore makes mergers

of the inner sub-Neptunes more likely. In general, a larger part of the parameter space is stable at larger \mathcal{P} but this trend would likely reverse when $\bar{\epsilon} \gtrsim 1$ ($\mathcal{P} \gtrsim 3.5$) and the influence of the giant planet becomes substantial.

If the sub-Neptune progenitors were close to a mean-motion resonance, they would easily undergo the mergers necessary to produce a planet such as Kepler-511 c. For \mathcal{P} not close to mean-motion resonances, the stability probability can be as high as 0.4–0.8 even when planet eccentricities are set by secular perturbation from Kepler-511 b. We note that 10^9 orbits of the innermost planet only correspond to ~ 70 Myr, which is a mere 1% of the system age. These stability probabilities should be treated as upper limits and they could be much lower over Gyr timescales (10^{11} orbits). Indeed, the median and 84th percentile instability times for orbital configurations with stability probability > 0.4 (when e is set by Kepler-511 b, dashed line in Figure 9) are lower than the age of the system (M. Cranmer et al. 2021). Mergers therefore provide a plausible albeit a low likelihood pathway for the formation of Kepler-511 c-like planets in some planetary systems, which would be commensurate with their low occurrence rates (see also D. Liveoak & S. C. Millholland 2024, for a similar mechanism to produce Neptune-like planets around very low mass stars).

The process by which Kepler-511 b came to acquire its significant eccentricity also might have played a role in destabilizing any inner planets that could coalesce to form Kepler-511 c. For example, if the outer unconfirmed companion scattered Kepler-511 b to its current orbit, such an event could have destabilized an inner system of sub-Neptunes. A more precise measurement of Kepler-511 c's eccentricity (our current estimate is consistent with zero) could provide more insight into its dynamical history and the plausibility of mergers as an origin channel for planets like Kepler-511 c.

The plausibility of this hypothesis also depends on the impact of mergers on the atmosphere retention of the final planet. The outcome of the merger on atmosphere loss depends on the mass ratio, impact velocity, and the geometry of the impact as well as the post-merger thermal evolution (E. Asphaug 2010; Z. M. Leinhardt & S. T. Stewart 2012; S. T. Stewart et al. 2014; N. K. Inamdar & H. E. Schlichting 2016; H. E. Schlichting & S. Mukhopadhyay 2018; J. B. Biersteker & H. E. Schlichting 2019). Since the probability of having an impact parameter $\leq b$ scales as b^2 , planets are much more likely to collide at oblique angles rather than head-on. In our scenario with $\sim 10 M_{\oplus}$ bodies, impact velocities in the range $\sim e_{\text{cross}} v_K - v_{\text{esc}}$ (v_K and v_{esc} are the Keplerian and mutual escape velocities; see also D. Liveoak & S. C. Millholland 2024 who find sub-escape impact velocities), and the higher likelihood of an oblique impact suggests that mergers will likely strip a small fraction of the atmosphere (T. R. Denman et al. 2020, 2022; L. Naponiello et al. 2023). We encourage continued exploration of the impact of mergers on envelope retention for the tightly packed close-in exoplanets.

6. Summary

In this work, we collected RV measurements of Kepler-511 over an 8.5 yr baseline (Figure 3) to dynamically confirm its two (previously validated) transiting exoplanets. Kepler-511 b is a gas giant planet with $M_p = 0.44^{+0.11}_{-0.12} M_J$ on a 297 days, moderately eccentric orbit. Given its unlikely transiting orbit, Kepler-511 b is a prime member of the GOT ‘EM survey (P. A. Dalba et al. 2021a, 2021b; C. R. Mann et al. 2023). Its inner ($P = 27$ days) companion (Kepler-511 c) has a mass of

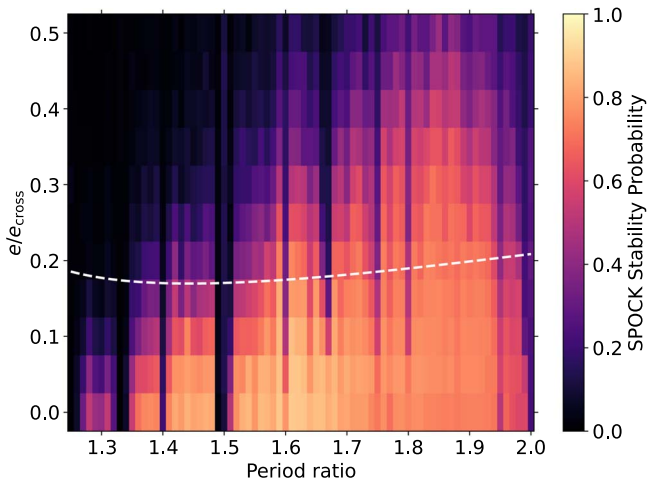


Figure 9. The stability probability for a system of three $10.5 M_{\oplus}$ planets with a given eccentricity (as a fraction of the crossing eccentricity) and period ratio accompanied by an outer giant with the properties of Kepler-511 b calculated by SPOCK. The dashed line indicates the rms time-averaged eccentricity of the three planets as a result of their interaction with the outer giant calculated via secular analytical theory.

$32^{+11}_{-12} M_{\oplus}$ and is three times as dense. We also identify a long-term trend in the RV time-series data that is most likely indicative of an additional massive object (planetary or otherwise) in the outer reaches of the Kepler-511 system (Section 3.3).

We take advantage of both planets’ relatively long orbits and low stellar irradiation (compared to other transiting exoplanets) to infer their bulk metallicities (Section 4.1). Interestingly, both planets have similar masses of heavy elements ($31^{+12}_{-10} M_{\oplus}$ and $26^{+11}_{-10} M_{\oplus}$ for planets b and c, respectively) but only Kepler-511 b seems to have accreted a massive gaseous envelope. Since the ability of planets to accrete primordial gas depends on their heavy element content, the Kepler-511 planets are an intriguing duo that poses an informative challenge to planet formation and evolution theories.

We explore three scenarios that could account for the planets’ current properties. First, we rule out envelope mass loss as a means to explain the difference in bulk metallicities of these planets: at 27 days, Kepler-511 c is simply too far away from its host star to suffer significant mass loss. Second, we evaluate a variety of reasons why their gas accretion histories might have differed. Although differences in the dust content of the disk gas accreted by these planets could drive their divergent accretion histories, it is difficult to attain such strong contrasts in the local dust content. Finally, we consider the scenario that Kepler-511 c is gas-poor because it formed from the merger of lower mass cores (that accrete less gas) after the dissipation of the protoplanetary disk. We show that secular perturbations from Kepler-511 b could pump up the eccentricities of such an inner system of sub-Neptunes and render their merger more likely over long timescales.

Overall, the Kepler-511 system serves as an important benchmark for numerous reasons. It contains multiple giant planets; both planets transit, enabling measurement of their radii; the outer planet has an exceptionally long orbital period considering its transiting geometry, leaving it with irradiation only 4.5 times that of Earth and an equilibrium temperature of ~ 400 K; and the two planets seem to have divergent accretion histories. We encourage additional theoretical explorations to

provide an explanation for how systems of multiple giant planets like Kepler-511 could have formed.

Acknowledgments

The authors recognize the cultural significance and sanctity that the summit of Maunakea has within the indigenous Hawaiian community. We are deeply grateful to have the opportunity to conduct observations from this mountain. We acknowledge the impact of our presence there and the ongoing efforts to preserve this special place.

The authors thank all of the observers in the California Planet Search team for their many hours of hard work in collecting the RVs published here. We thank an anonymous referee for their constructive comments, especially regarding the nature of the host star, that led us to sharpen our analysis. The authors are grateful to Jonathan Fortney, Sarah Millholland, and Yanqin Wu for helpful conversations about this planetary system. We are particularly indebted to Adam Kraus for an enlightening and extremely useful exchange on the possible binarity of this system. Part of this research was conducted at the Other Worlds Laboratory Summer Program 2022 at UC Santa Cruz, which is generously supported by the Heising-Simons Foundation. P.D. acknowledges support by a 51 Pegasi b Postdoctoral Fellowship from the Heising-Simons Foundation and by a National Science Foundation (NSF) Astronomy and Astrophysics Postdoctoral Fellowship under award AST-1903811. M.P. gratefully acknowledges NASA award 80NSSC22M0024.

This research has made use of the NASA Exoplanet Archive, which is operated by the California Institute of Technology, under contract with the National Aeronautics and Space Administration under the Exoplanet Exploration Program. This paper includes data collected by the Kepler mission and obtained from the MAST data archive at the Space Telescope Science Institute (STScI). Funding for the Kepler mission is provided by the NASA Science Mission Directorate. STScI is operated by the Association of Universities for Research in Astronomy, Inc., under NASA contract NAS 5-26555. This research has made use of the Exoplanet Follow-up Observation Program (ExoFOP; DOI:10.26134/ExoFOP5) website, which is operated by the California Institute of Technology, under contract with the National Aeronautics and Space Administration under the Exoplanet Exploration Program.

Some of the data presented herein were obtained at the W. M. Keck Observatory, which is operated as a scientific partnership among the California Institute of Technology, the University of California, and NASA. The Observatory was made possible by the generous financial support of the W. M. Keck Foundation. Some of the Keck data were obtained under PI Data awards 2013A and 2013B (M. Payne).

Facilities: Keck:I (HIRES), Kepler.

Software: *astropy* (Astropy Collaboration et al. 2013, 2018), *corner* (D. Foreman-Mackey 2016), *EXOFASTv2* (J. Eastman et al. 2013; J. Eastman 2017; J. D. Eastman et al. 2019), *lightkurve* (Lightkurve Collaboration et al. 2018), *RadVel* (B. J. Fulton et al. 2018) *SpecMatch* (E. A. Petigura 2015; E. A. Petigura et al. 2017), *pymc3* (J. Salvatier et al. 2016), *theano* (Theano Development Team et al. 2016), *REBOUND* (H. Rein & S. F. Liu 2012), *SPOCK* (D. Tamayo et al. 2020), *exoplanet* (E. Agol et al. 2020; D. M. Kipping 2013; D. Foreman-Mackey et al. 2021a, 2021b), *celerite2*

(D. Foreman-Mackey et al. 2017; D. Foreman-Mackey 2018),
starry (R. Luger et al. 2019), arviz (R. Kumar et al. 2019).

Appendix A

Limits on the Presence of a Companion from RV Spectra

We performed the `RealMatch` analysis laid out in R. Kolbl et al. (2015) on our RV spectra for Kepler-511. The results of

this analysis for two of our spectra are shown in Figure 10. We are sensitive to companions that are 1% the brightness of the primary and ΔRV separations of $\geq \pm 10 \text{ km s}^{-1}$. Within these limits, we do not detect any secondary companions. Although this analysis does not eliminate a nearly face-on equal mass companion directly, we present additional arguments that disfavor such a companion in Section 3.1.

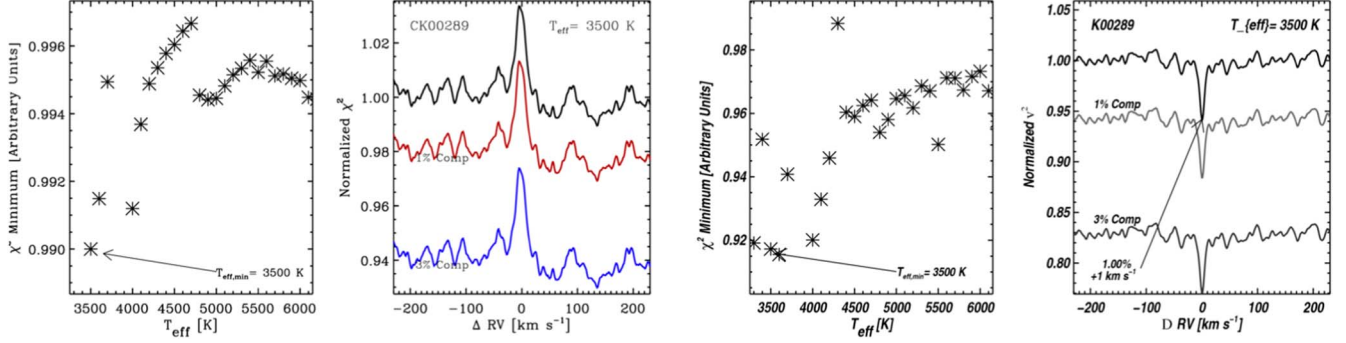


Figure 10. `RealMatch` analysis plots for two of our RV spectra (R. Kolbl et al. 2015). We rule out any secondary companions brighter than 1% of the primary’s brightness with an RV separation of $\geq \pm 10 \text{ km s}^{-1}$.

Appendix B

Fits with and without Stellar Density Constraints

Figure 11 shows the difference in log-likelihood of the fits to the RV and transit data with and without a prior on the stellar density. The higher log-likelihood for the fit without a prior on the stellar density is driven entirely by the RV data. The sparsely sampled RV data bias the fitted eccentricity and

argument of periastron, which in turn affects the fitted a/R_* from the transit data and the resulting stellar density (Figure 12). To mitigate this effect, N. Espinoza et al. (2019) recommend placing a prior on the stellar density instead. For planets with high eccentricities, this choice can also be used to better constrain their eccentricities via the “photoeccentricity” effect (R. I. Dawson & J. A. Johnson 2012).

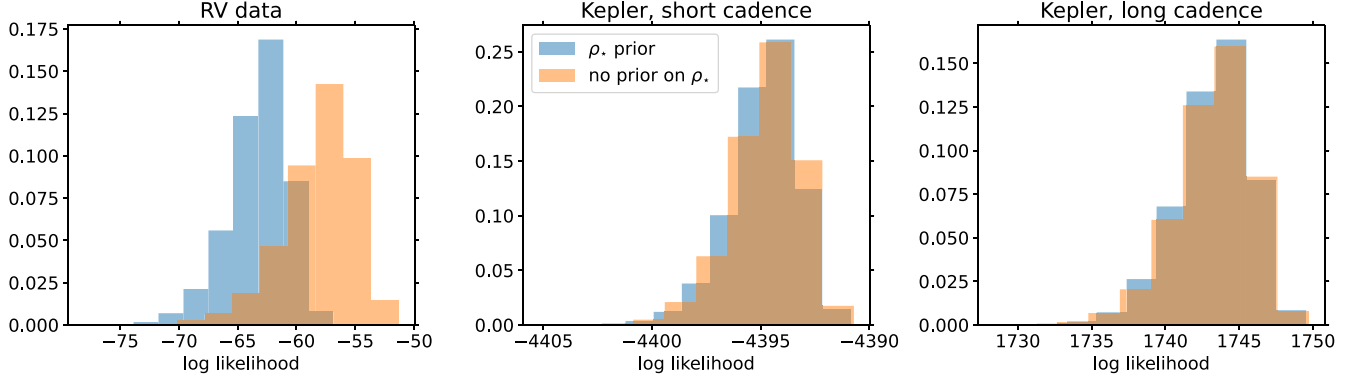


Figure 11. The histograms for log-likelihoods of our fits to the RV data and short cadence and long cadence transit data. The preference for a fit without a prior on the stellar density is driven by the RV data, which biases the fitted eccentricity and argument of periastron of Kepler-511 b.

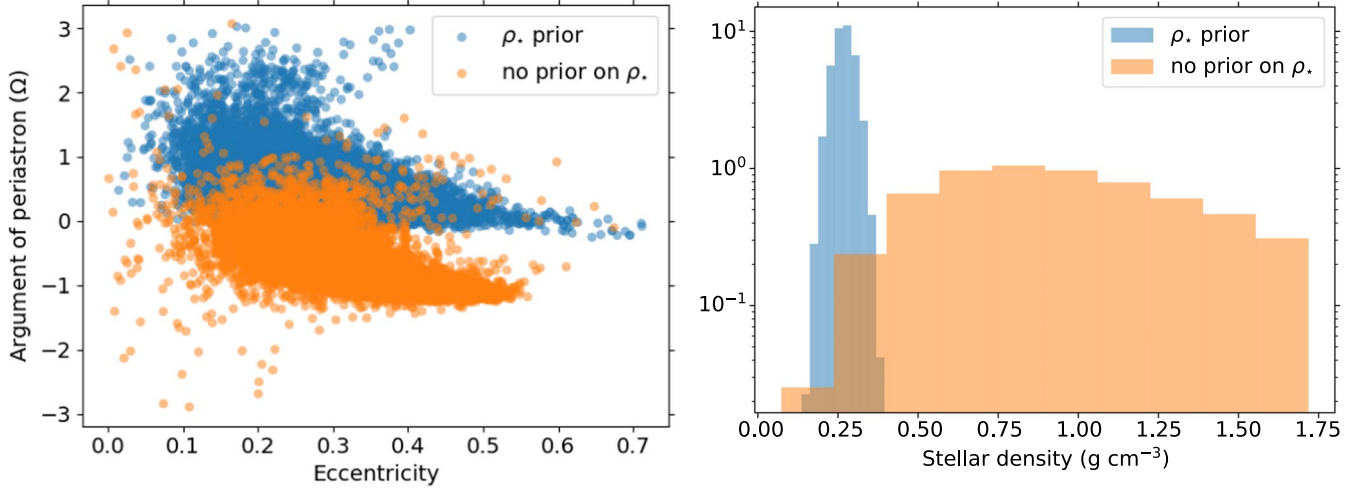


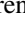



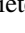




Figure 12. The left panel shows the fitted eccentricity and argument of periastron of Kepler-511 b with and without a prior on the stellar density. The right panel compares our stellar density prior with its fitted posterior when no prior is placed.

ORCID iDs

Yayaati Chachan  <https://orcid.org/0000-0003-1728-8269>
 Paul A. Dalba  <https://orcid.org/0000-0002-4297-5506>
 Daniel P. Thorngren  <https://orcid.org/0000-0002-5113-8558>
 Stephen R. Kane  <https://orcid.org/0000-0002-7084-0529>
 Howard Isaacson  <https://orcid.org/0000-0002-0531-1073>
 Eve J. Lee  <https://orcid.org/0000-0002-1228-9820>
 Edward W. Schwieterman  <https://orcid.org/0000-0002-2949-2163>
 Andrew W. Howard  <https://orcid.org/0000-0001-8638-0320>
 Matthew J. Payne  <https://orcid.org/0000-0001-5133-6303>

References

- Agol, E., Luger, R., & Foreman-Mackey, D. 2020, *AJ*, **159**, 123
 Akeson, R. L., Chen, X., Ciardi, D., et al. 2013, *PASP*, **125**, 989
 Ali-Dib, M., Cumming, A., & Lin, D. N. C. 2020, *MNRAS*, **494**, 2440
 Asplund, E. 2010, *ChEG*, **70**, 199
 Asplund, M., Amarsi, A. M., & Grevesse, N. 2021, *A&A*, **653**, A141
 Astropy Collaboration, Price-Whelan, A. M., Sipőcz, B. M., et al. 2018, *AJ*, **156**, 123
 Astropy Collaboration, Robitaille, T. P., Tollerud, E. J., et al. 2013, *A&A*, **558**, A33
 Bailey, A., & Zhu, Z. 2024, *MNRAS*, **534**, 2953
 Berger, T. A., Huber, D., van Saders, J. L., et al. 2020, *AJ*, **159**, 280
 Berger, T. A., Schlieder, J. E., & Huber, D. 2023, arXiv:2301.11338
 Bergez-Casalou, C., Bitsch, B., & Raymond, S. N. 2023, *A&A*, **669**, A129
 Biersteker, J. B., & Schlichting, H. E. 2019, *MNRAS*, **485**, 4454
 Bitsch, B., Morbidelli, A., Johansen, A., et al. 2018, *A&A*, **612**, A30
 Borsato, L., Degen, D., Leleu, A., et al. 2024, *A&A*, **689**, A52
 Borucki, W. J., Koch, D., Basri, G., et al. 2010, *Sci*, **327**, 977
 Boss, A. P. 1997, *Sci*, **276**, 1836
 Bressan, A., Marigo, P., Girardi, L., et al. 2012, *MNRAS*, **427**, 127
 Bryan, M. L., Knutson, H. A., Lee, E. J., et al. 2019, *AJ*, **157**, 52
 Butler, R. P., Marcy, G. W., Williams, E., et al. 1996, *PASP*, **108**, 500
 Butler, R. P., Vogt, S. S., Laughlin, G., et al. 2017, *AJ*, **153**, 208
 Caldiroli, A., Haardt, F., Gallo, E., et al. 2022, *A&A*, **663**, A122
 Carrera, D., Raymond, S. N., & Davies, B. 2019, *A&A*, **629**, L7
 Chachan, Y., & Lee, E. J. 2023, *ApJL*, **952**, L20
 Chachan, Y., Lee, E. J., & Knutson, H. A. 2021, *ApJ*, **919**, 63
 Chen, D.-C., Xie, J.-W., Zhou, J.-L., et al. 2021, *ApJ*, **909**, 115
 Chen, Y.-X., Li, Y.-P., Li, H., & Lin, D. N. C. 2020, *ApJ*, **896**, 135
 Choi, J., Dotter, A., Conroy, C., et al. 2016, *ApJ*, **823**, 102
 Cranmer, M., Tamayo, D., Rein, H., et al. 2021, *PNAS*, **118**, e2026053118
 Dai, F., Goldberg, M., Batygin, K., et al. 2024, *AJ*, **168**, 239
 Dalba, P. A., Kane, S. R., Li, Z., et al. 2021b, *AJ*, **162**, 154
 Dalba, P. A., Kane, S. R., Isaacson, H., et al. 2021a, *AJ*, **161**, 103
 Dalba, P. A., Kane, S. R., Isaacson, H., et al. 2024, *ApJS*, **271**, 16
 Dawson, R. I., & Johnson, J. A. 2012, *ApJ*, **756**, 122
 Dawson, R. I., Lee, E. J., & Chiang, E. 2016, *ApJ*, **822**, 54
 Denman, T. R., Leinhardt, Z. M., & Carter, P. J. 2022, *MNRAS*, **513**, 1680
 Denman, T. R., Leinhardt, Z. M., Carter, P. J., & Mordasini, C. 2020, *MNRAS*, **496**, 1166
 Díaz, R. F., Ségransan, D., Udry, S., et al. 2016, *A&A*, **585**, A134
 Dotter, A. 2016, *ApJS*, **222**, 8
 Drazkowska, J., Alibert, Y., & Moore, B. 2016, *A&A*, **594**, A105
 Duffell, P. C., & MacFadyen, A. I. 2013, *ApJ*, **769**, 41
 Dupuy, T. J., Kraus, A. L., Kratter, K. M., et al. 2022, *MNRAS*, **512**, 648
 Eastman, J. 2017, EXOFASTv2: Generalized Publication-quality Exoplanet Modeling Code, v2, Astrophysics Source Code Library, ascl:1710.003
 Eastman, J., Gaudi, B. S., & Agol, E. 2013, *PASP*, **125**, 83
 Eastman, J. D., Rodriguez, J. E., Agol, E., et al. 2019, arXiv:1907.09480
 Espinoza, N., Kossakowski, D., & Brahm, R. 2019, *MNRAS*, **490**, 2262
 Fischer, D. A., & Valenti, J. 2005, *ApJ*, **622**, 1102
 Foreman-Mackey, D. 2016, *JOSS*, **1**, 24
 Foreman-Mackey, D. 2018, *RNAAS*, **2**, 31
 Foreman-Mackey, D., Agol, E., Ambikasaran, S., & Angus, R. 2017, *AJ*, **154**, 220
 Foreman-Mackey, D., Luger, R., Agol, E., et al. 2021a, *JOSS*, **6**, 3285
 Foreman-Mackey, D., Savel, A., Luger, R., et al. 2021b, exoplanet-dev/exoplanet v0.5.1, Zenodo, doi:10.5281/zenodo.1998447
 Fortney, J. J., Marley, M. S., & Barnes, J. W. 2007, *ApJ*, **659**, 1661
 Fulton, B. J., Collins, K. A., Gaudi, B. S., et al. 2015, *ApJ*, **810**, 30
 Fulton, B. J., Petigura, E. A., Blunt, S., & Sinukoff, E. 2018, *PASP*, **130**, 044504
 Fung, J., Shi, J.-M., & Chiang, E. 2014, *ApJ*, **782**, 88
 Furlan, E., Ciardi, D. R., Everett, M. E., et al. 2017, *AJ*, **153**, 71
 Gaia Collaboration, Brown, A. G. A., Vallenari, A., et al. 2018, *A&A*, **616**, A1
 Gaia Collaboration, Prusti, T., de Bruijne, J. H. J., et al. 2016, *A&A*, **595**, A1
 Gaia Collaboration, Vallenari, A., Brown, A. G. A., et al. 2023, *A&A*, **674**, A1
 Goldreich, P., & Tremaine, S. 1980, *ApJ*, **241**, 425
 Griveaud, P., Crida, A., & Lega, E. 2023, *A&A*, **672**, A190
 Guillot, T., Santos, N. C., Pont, F., et al. 2006, *A&A*, **453**, L21
 Gundlach, B., Schmidt, K. P., Kreuzig, C., et al. 2018, *MNRAS*, **479**, 1273
 Hadden, S., & Lithwick, Y. 2018, *AJ*, **156**, 95
 Hasegawa, Y., Bryden, G., Ikoma, M., Vasisht, G., & Swain, M. 2018, *ApJ*, **865**, 32
 Holczer, T., Mazeh, T., Nachmani, G., et al. 2016, *ApJS*, **225**, 9
 Howard, A. W., Johnson, J. A., Marcy, G. W., et al. 2010, *ApJ*, **721**, 1467
 Ikoma, M., Emori, H., & Nakazawa, K. 2001, *ApJ*, **553**, 999
 Inamdar, N. K., & Schlichting, H. E. 2016, *ApJL*, **817**, L13
 Isaacson, H., & Fischer, D. 2010, *ApJ*, **725**, 875
 Jenkins, J. M., Caldwell, D. A., Chandrasekaran, H., et al. 2010, *ApJL*, **713**, L87
 Johnstone, C. P., Bartel, M., & Güdel, M. 2021, *A&A*, **649**, A96
 Kimura, H., Wada, K., Yoshida, F., et al. 2020, *MNRAS*, **1682**, 1667
 Kipping, D. M. 2013, *MNRAS*, **435**, 2152
 Kolb, R., Marcy, G. W., Isaacson, H., & Howard, A. W. 2015, *AJ*, **149**, 18
 Kraus, A. L., Ireland, M. J., Huber, D., Mann, A. W., & Dupuy, T. J. 2016, *AJ*, **152**, 8
 Kumar, R., Carroll, C., Hartikainen, A., & Martin, O. A. 2019, *JOSS*, **4**, 1143
 Lammers, C., Hadden, S., & Murray, N. 2024, *ApJ*, **972**, 53
 Lee, E. J., & Chiang, E. 2015, *ApJ*, **811**, 41
 Lee, E. J., & Chiang, E. 2016, *ApJ*, **817**, 90
 Lee, E. J., & Connors, N. J. 2021, *ApJ*, **908**, 32
 Lee, J.-M., Irwin, P. G. J., Fletcher, L. N., Heng, K., & Barstow, J. K. 2014, *ApJ*, **789**, 14
 Leinhardt, Z. M., & Stewart, S. T. 2012, *ApJ*, **745**, 79
 Lightkurve Collaboration, Cardoso, J. V. d. M., Hedges, C., et al. 2018, Lightkurve: Kepler and TESS Time Series Analysis in Python, 1.11, Astrophysics Source Code Library, ascl:1812.013
 Lindegren, L., Klioner, S. A., Hernández, J., et al. 2021, *A&A*, **649**, A2
 Lithwick, Y., & Naoz, S. 2011, *ApJ*, **742**, 94
 Liveoak, D., & Millholland, S. C. 2024, *ApJ*, **974**, 207
 Lodders, K. 2021, *SSRv*, **217**, 44
 Lopez, E. D., Fortney, J. J., & Miller, N. 2012, *ApJ*, **761**, 59
 Lovis, C., Dumusque, X., Santos, N. C., et al. 2011, arXiv:1107.5325
 Luger, R., Agol, E., Foreman-Mackey, D., et al. 2019, *AJ*, **157**, 64
 Mann, C. R., Dalba, P. A., Lafrenière, D., et al. 2023, *AJ*, **166**, 239
 Miguel, Y., Guisler, O. M., & Brunini, A. 2011, *MNRAS*, **417**, 314
 Miguel, Y., Guillot, T., & Fayon, L. 2016, *A&A*, **596**, A114
 Moldenhauer, T. W., Kuiper, R., Kley, W., & Ormel, C. W. 2021, *A&A*, **646**, L11
 Morton, T. D., Bryson, S. T., Coughlin, J. L., et al. 2016, *ApJ*, **822**, 86
 Mousis, O., Marboeuf, U., Lunine, J. I., et al. 2009, *ApJ*, **696**, 1348
 Musiolik, G., & Wurm, G. 2019, *ApJ*, **873**, 58
 Naponiello, L., Mancini, L., Sozzetti, A., et al. 2023, *Natur*, **622**, 255
 Öberg, K. I., Murray-Clay, R., & Bergin, E. A. 2011, *ApJL*, **743**, L16
 Ormel, C. W. 2014, *ApJL*, **789**, L18
 Ormel, C. W., Shi, J.-M., & Kuiper, R. 2015, *MNRAS*, **447**, 3512
 Paxton, B., Bildsten, L., Dotter, A., et al. 2011, *ApJS*, **192**, 3
 Paxton, B., Cantiello, M., Arras, P., et al. 2013, *ApJS*, **208**, 4
 Paxton, B., Marchant, P., Schwab, J., et al. 2015, *ApJS*, **220**, 15
 Penoyre, Z., Belokurov, V., Wyn Evans, N., Everall, A., & Koposov, S. E. 2020, *MNRAS*, **495**, 321
 Petigura, E. A. 2015, PhD thesis, Univ. of California, Berkeley
 Petigura, E. A., Howard, A. W., Marcy, G. W., et al. 2017, *AJ*, **154**, 107
 Petit, A. C., Pichierr, G., Davies, M. B., & Johansen, A. 2020, *A&A*, **641**, A176
 Piso, A.-M. A., Youdin, A. N., & Murray-Clay, R. A. 2015, *ApJ*, **800**, 82
 Pollack, J. B., Hubickyj, O., Bodenheimer, P., et al. 1996, *Icar*, **124**, 62
 Poon, S. T. S., & Nelson, R. P. 2020, *MNRAS*, **498**, 5166
 Pu, B., & Lai, D. 2018, *MNRAS*, **478**, 197
 Pu, B., & Wu, Y. 2015, *ApJ*, **807**, 44
 Rafikov, R. R. 2006, *ApJ*, **648**, 666

- Rasio, F. A., & Ford, E. B. 1996, *Sci*, **274**, 954
- Rein, H., & Liu, S. F. 2012, *A&A*, **537**, A128
- Rosenthal, L. J., Fulton, B. J., Hirsch, L. A., et al. 2021, *ApJS*, **255**, 8
- Salvatier, J., Wiecki, T. V., & Fonnesbeck, C. 2016, *PeerJ Comput. Sci.*, **2**, e55
- Savignac, V., & Lee, E. J. 2024, *ApJ*, **973**, 85
- Schlafly, E. F., & Finkbeiner, D. P. 2011, *ApJ*, **737**, 103
- Schlichting, H. E., & Mukhopadhyay, S. 2018, *SSRv*, **214**, 34
- Smith, J. C., Stumpe, M. C., Van Cleve, J. E., et al. 2012, *PASP*, **124**, 1000
- Sobski, N., & Millholland, S. C. 2023, *ApJ*, **954**, 137
- Stevenson, D. J. 1982, *P&SS*, **30**, 755
- Stewart, S. T., Lock, S. J., & Mukhopadhyay, S. 2014, *LPSC*, **45**, 2869
- Stumpe, M. C., Smith, J. C., Van Cleve, J. E., et al. 2012, *PASP*, **124**, 985
- Tamayo, D., Cranmer, M., Hadden, S., et al. 2020, *PNAS*, **117**, 18194
- Tayar, J., Claytor, Z. R., Huber, D., & van Saders, J. 2022, *ApJ*, **927**, 31
- Theano Development Team, Al-Rfou, R., Alain, G., et al. 2016, arXiv:1605.02688
- Thompson, S. E., Coughlin, J. L., Hoffman, K., et al. 2018, *ApJS*, **235**, 38
- Thorngren, D., & Fortney, J. J. 2019, *ApJL*, **874**, L31
- Thorngren, D. P., Fortney, J. J., Murray-Clay, R. A., & Lopez, E. D. 2016, *ApJ*, **831**, 64
- Thorngren, D. P., Lee, E. J., & Lopez, E. D. 2023, *ApJL*, **945**, L36
- Torres, G., Fischer, D. A., Sozzetti, A., et al. 2012, *ApJ*, **757**, 161
- Tsiganis, K., Gomes, R., Morbidelli, A., & Levison, H. F. 2005, *Natur*, **435**, 459
- Valizadegan, H., Martinho, M. J. S., Wilkens, L. S., et al. 2022, *ApJ*, **926**, 120
- Vogt, S. S., Allen, S. L., Bigelow, B. C., et al. 1994, *Proc. SPIE*, **2198**, 362
- Walsh, K. J., Morbidelli, A., Raymond, S. N., O'Brien, D. P., & Mandell, A. M. 2011, *Natur*, **475**, 206
- Winn, J. N., Albrecht, S., Johnson, J. A., et al. 2011, *ApJL*, **741**, L1
- Wisdom, J. 1980, *AJ*, **85**, 1122
- Woitke, P., Helling, C., Hunter, G. H., et al. 2018, *A&A*, **614**, A1
- Wright, J. T., Marcy, G. W., Butler, R. P., & Vogt, S. S. 2004, *ApJS*, **152**, 261
- Wu, Y., & Murray, N. 2003, *ApJ*, **589**, 605
- Zhu, W. 2022, *AJ*, **164**, 5
- Zhu, W., & Wu, Y. 2018, *AJ*, **156**, 92
- Zhu, Z., Jiang, Y.-F., Baehr, H., et al. 2021, *MNRAS*, **508**, 453